Modelling and Design of Millimeter-Wave Networks for Highway Vehicular Communication

Andrea Tassi, Malcolm Egan, Robert J. Piechocki and Andrew Nix

***Abstract*—onnected and autonomous vehicles will play a pivotal role in future Intelligent Transportation Systems (ITSs) and smart cities, in general. High-speed and low-latency communication links will allow municipalities to inform vehicles of safety hazards, as well as support cloud-driving solutions to reduce traffic jams and air pollution.onnected and autonomous vehicles will play a pivotal role in future Intelligent Transportation Systems (ITSs) and smart cities, in general. High-speed and low-latency communication links will allow municipalities to inform vehicles of safety hazards, as well as support cloud-driving solutions to reduce traffic jams and air pollution.C This requires vehicles that carry a large number of sensors that exchange high data rate sensor row-data streams. Recently, millimeter wave (mmWave) techniques have been introduced as a means of achieving such high data rate streams. In this paper, we model of a highway communication network for characterizing fundamental link budged metrics. We specifically consider the case where vehicles are served by mmWave Base Stations (BSs) on the side of the road. To evaluate our highway network, we develop a new model that accounts for the common scenario where vehicles (such as buses and lorries) in slow lanes block Line-of-Sight (LOS) paths to vehicles in fast lanes and, hence, behave as blockages. Using tools from stochastic geometry, we derive approximations for the Signal-to-Interference-plus-Noise ratio (SINR) outage probability, as well as the probability that a user achieves a target communication rate (rate coverage probability). We show via a comparison with Monte Carlo simulations that our approximations capture key trends in the SINR outage and rate coverage probabilities. We also provide design insights for mmWave highway communication networks. In particular, we show that smaller antenna beamwidths and, unlike bi-dimensional mmWave cellular networks, smaller BS densities do not necessarily have a disruptive impact on improving the SINR outage probability, and hence on improving the rate coverage probability.**

***Index Terms*—Vehicular communications, millimeter-wave networks, performance modelling, stochastic geometry.**

I. Introduction

By 2020, fifty billion devices will have connectivity capabilities [1]. Among these, ten million vehicles equipped with on-board communication systems and with a range of autonomous capabilities will be progressively rolled out [2]. According to the National Highway Traffic Safety Administration (U.S. Department of Transportation) and the European Commission's Connected-Intelligent Transportation System (C-ITS) initiative [3], [4], connectivity will allow vehicles to deeply engage with future ITS services. For instance, semi-autonomous (level 3 of SAE J3016 [5]) or fully-autonomous (levels 4-5 of SAE J3016) vehicles will delegate all the cruise-control functionalities to the cloud - thus enabling distributed control centres to remotely drive each vehicle. As such, traffic jams and air pollution can be reduced. In addition, high-speed and low-latency communication links will allow virtually any connected vehicle to get access to live video feeds of the road ahead - thus making overtaking vehicles hazard-free [6].

As foreseen by the European Commission's C-ITS initiative, the set of sensors mounted on each vehicle has increased and are expected to range from ultra-sound proximity sensors to more complicated camcorders and 'Light Detection And Ranging' (LIDAR) systems [6]. Currently, the number of on-board sensors are around 100 units but this number is due to double by 2020 [7]. Ideally, the higher the number of on-board sensors, the "smarter" the vehicle. Unfortunately, this is true only if vehicles can exchange what they locally sense [8]. Consider the case where multiple LIDAR-equipped vehicles are close to a road hazard and share their real-time LIDAR data with approaching vehicles, via road-side infrastructure. This allows the approaching vehicles to integrate their lack of sensor data (blind-spot removal) and, for instance, improve the decisions performed by their smart cruise-control systems. This imposes strong constraints on the communications system. For example, vehicular radar (for target detection) generates approximately $1\,\mathrm{Mbps}$ and a typical set of camcorders generates $90\,\mathrm{Mbps}$ of compressed video feeds [9]. Moreover, semi- and full-autonomous vehicles are likely to be equipped with LIDAR systems, which can generate up to $100\,\mathrm{Mbps}$ of data.

Table. I summarizes the main technologies that have been considered to enable Infrastructure-to-Vehicle (I2V) communications in ITSs. Traditionally, ITSs have been based on Dedicated Short-Range Communication (DSRC) standards. The most commonly adopted standards in the DSRC class are the IEEE 802.11p/DSRC or the ITS-G5/DSRC [10]–[13]. Even though these standard operate in a licensed band and ensure low communication latencies, their maximum realistic data rate barely exceeds $6\,\mathrm{Mbps}$ [10]. As such, several papers [14], [15] propose the adoption of Long Term Evolution-Advanced (LTE-A), which enables larger data rates. Unfortunately, despite its MIMO capabilities, LTE-A systems can only support a maximum data rate of $100\,\mathrm{Mbps}$. In addition, LTE-A systems usually require radio resources to be centrally allocated by the core network - thus making it hard to guarantee end-to-end latencies smaller than $100\,\mathrm{ms}$ [8]. As noted in the 5G-PPP's communication requirements for future ITS services [6],

A. Tassi, R. J. Piechocki and A. Nix are with the Department of Electrical and Electronic Engineering, University of Bristol, UK (e-mail: {a.tassi,r.j.piechocki,Andy.Nix}@bristol.ac.uk).

M. Egan is with the Laboratoire de Mathématiques, UMR 6620 CNRS, Université Blaise Pascal, Clermont-Ferrand, FR (e-mail: malcolm.egan@math.univ-bpclermont.fr).

TABLE I
RADIO ACCESS SOLUTIONS FOR VEHICULAR COMMUNICATIONS.

	IEEE 802.11p/DSRC, ITS-G5/DSRC [13]	**LTE-A** [15]	**mmWave Systems** [16]
Frequency Band	5.85 GHz - 5.925 GHz	Spanning multiple bands in 450 MHz - 4.99 GHz	28 GHz, 38 GHz, 60 GHz bands and E-band
Channel Bandwidth	10 MHz	Up to 100 MHz	100 MHz-2.16 GHz
Bit Rate	3 Mbps-27 Mbps	Up to 1 Gbps	Up to 7 Gbps
Latency	≤ 10 ms	100 ms-200 ms	≤ 10 ms
Mobility Support	$\leq 130\,\mathrm{km\,h^{-1}}$	$\leq 350\,\mathrm{km\,h^{-1}}$	$\leq 100\,\mathrm{km\,h^{-1}}$
MIMO	Not supported	$\leq 8 \times 8$ in downlink and $\leq 4 \times 4$ in uplink	$\geq 10 \times 10$

semi-autonomous and fully-autonomous vehicles will require communication links capable of several gibabit-per-second and ensuring latencies of 10 ms or less, to support the exchange of sensor data [9].

Recently, communication systems operating in the millimeter-wave (mmWave) range of the spectrum have been proposed as a means of overcoming the limitations of existing IEEE 802.11p/DSRC and LTE-A standards [9], [17]. Generally, mmWave systems operate in the fraction of the spectrum between 30 GHz and 300 GHz and organize transmissions onto channels with bandwidths up to 2.16 GHz [16]. A key aspect of a mmWave system is that line-of-sight (LOS) communications are characterized by path loss exponents that tend to be smaller than 2.8, while non-line-of-sight (NLOS) may present much higher path loss exponents. Moreover, mmWave communications can be highly sensitive to blockages, leading to a NLOS path loss exponent equal to or greater than 3.8 [18]. Table I summarizes the general performance characteristics of mmWave compared with DSRC and LTE-A.

Consider the mobility support as in Table. I; both DSRC and LTE-A systems currently outperform mmWave system. However, in mmWave systems, both the BSs and the users are equipped with large antenna arrays to achieve high array gains via beamforming techniques [19]. Research in the topics of beamforming and beam searching is gaining momentum and it is reasonable to expect mmWave systems to develop improved mobility [20].

In this paper, we consider typical road-side infrastructure for ITSs [21]. As such, the infrastructure-to-vehicle (I2V) network interactions required by ITS services are handled by a dedicated network composed of Base Stations (BSs) placed at the sides of the road - thus BSs are fitted at the top of lampposts and other roadside locations, typically on both sides of the road [22], [23]. In particular, we deal with a highway system where vehicles are targeted by high data rate streams that are transmitted by mmWave BSs. A key feature of our highway system is that vehicles with different sizes are likely to drive along the same set of lanes. In a left-hand traffic system, any slow vehicle (such as double decker buses or lorries) typically travels in the outermost lanes of the highway, while the other vehicles tend to drive along the innermost lanes. As a consequence, if a large and tall vehicle drives between a user and its serving BS, this means that the BS is no longer in LOS. In other words, large vehicles may act as communication blockages.

The goals of this paper are twofold: (i) to provide an analytical characterization of the network coverage in a highway scenario, and (ii) to provide design insights that take into account how the BS and blockage densities impact the user Signal-to-Interference-plus-Noise Ratio (SINR) and achievable data rate. In particular, our performance analysis assesses the impact that the antenna gain and directivity have on the overall user performance. Since our analytical characterization establishes a link between the user performance, the traffic conditions and the mmWave network deployment characteristics, this provides a means of predicting user performance as he/she drives in scenarios that may involve different BS densities, traffic intensities, etc. It is beyond the scope of this paper to consider scenarios where there is no mmWave coverage or where the mmWave BSs do not follow the road-side deployment approach, which can potentially be dealt with via vehicle-to-vehicle communication technologies.

A. Related Work and Paper Contributions

Recently, mmWave systems have been proposed as a viable alternative to traditional wireless local area networks [24] or as a way to implement wireless backhauling among BSs of the same cellular network [25], [26]. Furthermore, the application of mmWave technology has also been considered for deploying dense cellular networks characterized by high data rates [27]–[29]. With regards to the vehicular communication domain, J. Choi *et al.* [9], along with S. Takahashi *et al.* [30], pioneered the possibility of adopting mmWave technology to partially or completely enable ITS communications. A mmWave approach to ITS communications is also being supported by the European Commission, which recently foresaw the possibility of designing ITSs that rely on mmWave technology, and operating in the band spanning 63–64 GHz [4].

This papers relies on stochastic geometry tools for characterizing the SINR and rate coverage probabilities [31]. The idea of using stochastic geometry results for characterizing wireless network performance requires the modelling of the positions of transmitters to follow a Poisson Point Process (PPP). As such, these analytical tools allow us to make the performance model more general, as we are not required to specify the position of each BS but only their spatial density. As a result, the SINR is treated as a random variable and its distribution can be derived or at least approximated. This is particularly important in our system model, as it would be unrealistic to assume that mmWave BSs were placed in equally spaced locations. By exploiting the stochastic geometry results, our model can describe a more "casual" network deployment, which may be determined by physical road obstacles (i.e., overpasses preventing the installation of any BSs, etc.). Under the assumption that the locations of the BSs are distributed according to a homogeneous PPP, each user will experience network conditions with the same statistics, reducing the need to account explicitly for user mobility.

Generally, the stochastic geometry tools define a well established methodology for characterizing the performance of wireless networks [17], [31]–[35]. However, as noted in [27], it is not possible to directly apply traditional stochastic geometry results for the characterization of mmWave networks. This is because of the lack of theoretical frameworks able to take into account the distribution of blockages. Despite this, the presence of blockages has only been addressed in the context of mmWave cellular networks in urban and sub-urban environments [27]. Furthermore, traditional stochastic geometry frameworks assume that the BSs are distributed according to homogeneous bi-dimensional PPPs, which does not apply to our model. To the best of our knowledge, no stochastic geometry models for road-side mmWave BS deployment have been proposed to date. As such, in order to keep our analysis comparable with traditional stochastic geometry frameworks, we will refer to scenarios where BSs follows a mono-dimensional PPP. Despite the simplicity and tractability of the model, we will observe that this results in a non-trivial behavior of user performance and new design insights.

Given the simplicity of their topology and their high level of automation, highway scenarios have been well investigated [36]–[38]. In particular, [36] addresses the issue of optimizing the density of fixed transmitting nodes placed at the side of the road, with the objective of maximizing the stability of reactive routing strategies for Vehicular Ad-Hoc Networks (VANETs) based on the IEEE 802.11p/DSRC stack. While [37] proposes a performance investigation along the same track as [36], it describes a performance framework that jointly combines physical and Media Access Control (MAC) layer quality metrics. In contrast to [36] and [37], [38] addresses the issue of blockage-effects caused by large surrounding vehicles. However, the approach in [38] assumes an IEEE 802.11p/DSRC communication system. Moreover, the proposals in [36]–[38] are not applicable for mmWave highway networks as the propagation conditions of a mmWave communication system are not comparable with that characterizing a system operating between $5.855\,\mathrm{GHz}$ and $5.925\,\mathrm{GHz}$. Another fundamental difference is given by the fact that we assume that both transmitting and receiving nodes are equipped by antenna arrays capable of beamforming, while the IEEE 802.11p/DSRC stack strictly refers to omnidirectional or non-steering sectorial antennas. Hence, the distribution of the interference contribution of a mmWave system is indeed different compared to that of a traditional DSRC system.

In the track of the stochastic geometry and perhaps the work most related to our paper, M. J. Farooq *et al.* [39] propose a stochastic geometry model for highway vehicular communications. In particular, [39] considers a system that resembles the physical and MAC layers of IEEE 802.11p/DSRC or ITS-G5/DSRC. As such, the access to the medium is regulated by the Carrier Sense Multiple Access (CSMA) protocol. In addition, antennas are strictly omnidirectional and all transmissions occur in LOS. The fundamental objective of [39] is to provide a tractable framework for characterizing multi-hop inter-vehicle communications in highway scenarios - as such defining optimal traffic aggregation and forwarding techniques. In particular, the authors introduce the Aggregate Packet Progress (APP) metric, which is a dimensionless index of the average number of hops (normalized with respect to the road length) that a packet has to traverse to be successfully received by its final destination. Consider the CSMA carrier sensing threshold, the lower it is, the larger the distance between concurrent transmitters - thus reducing the interference at the expense of spatial frequency reuse efficiency. The APP metric is used to optimize the carrier sensing threshold and hence, to find a tradeoff between interference reduction and spatial frequency reuse efficiency. The APP metric is also used to compare the performance of the presented forwarding strategies. Despite the similarity with our system model, [39] refers to a completely different set of assumptions and aims to meet a very different set of goals. In particular, [39] differs from this paper since: (i) it focuses on multi-hop inter-vehicle communications and routing strategies while our paper deals with one-hop I2V coverage issues, (ii) it refers to communication devices with no beamforming capabilities while beamforming is key in our mmWave system, and (iii) it does not considered the possibility of having NLOS communications, which is a substantial part of our analysis. For these reasons, the SINR coverage model as in [39] is not applicable to our system model.

The approach in [27] currently forms the most comprehensive framework for the analysis and design of mmWave networks. However, the focus of [27] is on urban/suburban mmWave cellular networks that have key differences with highway mmWave networks. In particular, in cellular mmWave networks: (i) the positions of BSs follows a bi-dimensional PPP, and (ii) the positions of blockages are governed by a stationary and isotropic process. Even though this is a commonly accepted assumption for bi-dimensional cellular networks [31], these assumptions are not satisfied in highway scenarios, where both the blockages and the BS distributions are clearly not invariant to rotations or translations. As such, a different approach is required.

The main contributions and design insights of this paper are summarized as follows:

- We propose a stochastic geometry framework for characterizing the performance of a mmWave network, which provides downlink connectivity to users driving along the fastest lanes of an highway section;
- We show that the performance of mmWave highway networks can be accurately modelled by assuming that both BS and blockage positions are governed by multiple independent mono-dimensional PPPs with none of the processes invariant to translations and rotations. This allows for the assessment of the impact of road layout and traffic density on the SINR outage and rate coverage probabilities.
- We show that a smaller antenna beamwidth does not necessarily reduce the SINR outage probability;
- We show that the SINR outage probability in highway mmWave networks is minimized by low density BS deployments, for a fixed probability threshold.

The reminder of the paper is organized as follows. Section II

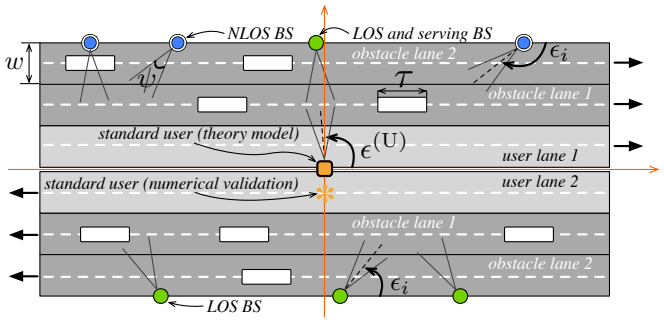

Fig. 1. Considered highway system model, composed by $N_o = 2$ obstacle lanes in each traffic direction.

presents our mmWave communication system downlink coverage in highway mmWave networks. We evaluate network performance in terms of SINR outage and rate coverage probabilities, which are derived in Section III. Section IV validates our theoretical model and investigates the impact of road layout, traffic density, BS density and antenna beamwidth on our performance metrics. In Section V, we conclude and outline avenues of future research.

II. System Model and Proposed BS-Standard User Association Paradigm

We consider a system model where mmWave BSs provide network coverage over a section of an highway. The goal of our performance model is to characterize the coverage probability of a user surrounded by several moving blockages (i.e., other vehicles) that may prevent a target user to be in LOS with the serving BS. Without loss of generality, we consider the scenario where vehicles drive on the left hand side of the road[1]. Fig. 1 illustrates the considered highway system model. In order to gain insight into the behavior of the model, we make the following set of assumptions. For clarity, Table II summarizes the symbols commonly used in the paper.

Assumption 2.1 (Road Layout): We assume that the whole road section is constrained within two infinitely long parallel lines, the *upper* and *bottom sides* of the considered road section. Vehicles flow along multiple parallel lanes in only two possible directions: West-to-East (for the upper-most lanes) and East-to-West (for the lowermost lanes). Each lane has the same width w. For each direction, there are N_o obstacle lanes and one user lane closer to the innermost part of the road. The closer a lane is to the horizontal symmetry axis of the road section, the more the average speed is likely to increase - thus, the large/tall vehicles are assumed to drive along obstacle lanes most of the time. Vehicles move along the horizontal symmetry axis of each lane. We use a coordinate system centered on a point on the line separating the directions of traffic. The upper side of the road intercepts the y-axis of our system of coordinates at the point $(0, w(N_o+1))$, while the bottom side intercepts at $(0, -w(N_o+1))$.

[1]Both the considered system model and the proposed theoretical framework can be easily extended to road systems where drivers are required to drive on the right hand side of the road.

TABLE II
Commonly used notation.

N_o	Number of obstacle lanes per driving direction
w	Width of a road lane
λ_{BS}	Density of the PPP Φ_{BS} of x-components of the BS locations on the road
$\lambda_{O,\ell}$	Density of the PPP $\Phi_{\mathrm{O},\ell}$ of x-components of the blockages on the ℓ-th obstacle lane
τ	Footprint segment of each blockage
p_{L}, p_{N}	Approximated probabilities of a BS being in LOS or NLOS with respect to the standard user, respectively
λ_{L}, λ_{N}	Densities of the PPPs of the x-components of LOS and NLOS BSs, respectively
$\ell(r_i)$	Path loss component associated with the i-th BS
A_{L}	Assuming the standard user connects to a NLOS BS at a distance r, it follows that there are no LOS BSs at a distance less or equal to $A_{\mathrm{L}}(r)$
A_{N}	Assuming the standard user connects to a LOS BS at a distance r, it follows that there are no NLOS BSs at a distance less or equal to $A_{\mathrm{N}}(r)$
$\mathrm{P_L}$, $\mathrm{P_N}$	Probabilities that the standard user connects to a LOS or a NLOS BS, respectively
G_{TX}, G_{RX}	Maximum transmit and receive antenna gains, respectively
g_{TX}, g_{RX}	Minimum transmit and receive antenna gains, respectively
$\mathcal{L}_{\mathrm{I}_{\mathrm{S,E}},\mathbb{E}_1}(s)$	Laplace transform of the interference component determined by BSs placed on the upper (S = U) or bottom side (S = B) of the road that are in LOS (E = L) or in NLOS (E = N) to the standard user, conditioned on $\mathbb{E}_1$ on the serving BS being in LOS ($\mathbb{E}_1$ = L) or NLOS ($\mathbb{E}_1$ = N)
$\mathcal{L}_{\mathrm{I},\mathbb{E}_1}(s)$	Laplace transform of the interference I, given that the standard user connects to a LOS BS ($\mathbb{E}_1$ = L) or NLOS BS ($\mathbb{E}_1$ = N)
$\mathrm{P_T}(\theta)$	SINR outage probability as a function of SINR threshold θ
$\mathrm{R_C}(\kappa)$	Rate coverage probability as a function of target rate κ

In the following sections, we will focus on characterizing the performance of the downlink phase of a mmWave cellular network providing connectivity to the vehicles flowing in the high speed lanes of the considered model. The performance characterization in this scenario is highly conservative. In particular, communication links targeting users in the high speed lanes are impacted by the largest number of communication blockages (namely, large/tall vehicles) flowing on on the outer road lanes.

Since mmWave technologies for ITS applications are a relatively new research topic, to the best of our knowledge we are not aware of any large-scale urban or highway cellular deployment currently running with this technology. As such, our analysis cannot directly refer to any existing mmWave network. Moreover, there is a need for basic design strategies for large-scale highway mmWave networks. To this end, we adopt the standard assumption of BS locations distributed according to a PPP, which is typical in the field of stochastic geometry.

Assumption 2.2 (BS Distribution): Let $\Phi_{\mathrm{BS}} = \{x_i\}_{i=1}^{b}$ be the one-dimensional PPP, with density λ_{BS} of the x-components of the BS locations on the road. We assume that BSs are located along with the upper and bottom sides of the road section. In particular, the i-th BS lies on the upper or bottom sides with a probability equal to $q = 0.5$. In other words, the y-axis coordinate of the i-th BS is defined as $y_i = w(-2\mathbb{B}_q+1)(N_o+1)$, where $\mathbb{B}_q$ is a Bernoulli random variable with parameter q.

By Assumption 2.2 and from the independent thinning theorem of PPP [40, Theorem 2.36], it follows that the x-axis coordinates of the BSs at the upper and bottom sides of the road form two independent PPPs with density $q\lambda_{\mathrm{BS}}$ or equally,

$(1-q)\lambda_{\rm BS}$.

Assumption 2.3 (Blockage Distribution): Considering the ℓ-th obstacle lane on a traffic direction and the coordinates $(x^{(\rm o)}_{\ell,i}, y^{(\rm o)}_{\ell,i})$ of blockage i, $x^{(\rm o)}_{\ell,i}$ belongs to a one-dimensional PPP $\Phi_{{\rm O},\ell}$ with density $\lambda_{{\rm o},\ell}$, for $\ell \in \{1,\ldots,N_o\}$ [39]. Term $y^{(\rm o)}_{\ell,i}$ is equal to $w\ell$, or $-w\ell$, depending on whether we refer to the West-to-East or East-to-West direction, respectively. We assume that the density of the blockage of lane ℓ in each traffic direction is the same. Each blockage point is associated with a segment of length τ, centred on the position of the blockage itself and placed onto the horizontal symmetry axis of the lane (hereafter referred to as the "footprint segment"). Obstacles can be partially overlapped and the blockage widths and heights are not be part of our modelling. The presence of large vehicles in the user lanes is regarded as sporadic and their impact on the user performance negligible - thus it is ignored.

From Assumption 2.3, given a driving direction, we observe that the blockage density of each obstacle lane can be different. This means that our model has the flexibility to consider different traffic levels per obstacle lane - namely, the larger the traffic density, the larger the traffic intensity.

Our primary goal is that of characterizing the SINR outage and rate coverage probability of users moving along the user lanes, as these are the most challenging to serve due to the fact that vehicles in the other lanes can behave as blockages. In order to keep our theoretical model tractable, the remainder of the paper will consider the service of a *standard user* placed at the origin $O=(0,0)$ of the axis. We observe that in Section IV, our theoretical model is validated with users placed at the center of one of the user lanes, i.e., we simulate with users placed at the point $(0,-w/2)$.

A. BS-Standard User Association and Antenna Model

Since vehicles in the slow lanes can block a direct link between the standard user and each BS, it is necessary to distinguish between BSs that are in LOS with the standard user and those that are in NLOS. The BS i is in LOS if the footprint of any blockage does not intersect with the direct ray from the standard user; we say that this occurs with probability $p_{i,{\rm L}}$. We assume the blockage is of length τ, which is illustrated in Fig. 1. In the case that the direct ray is blocked, the BS i is in NLOS and this occurs with probability $p_{i,{\rm N}}$ and the relation $p_{i,{\rm N}} = 1 - p_{i,{\rm L}}$ holds. By Assumption 2.3, observe that the probability $p_{i,{\rm E}}$ for ${\rm E} \in \{{\rm L},{\rm N}\}$ of BS i of being in LOS (${\rm E}={\rm L}$) or NLOS (${\rm E}={\rm N}$) depends on the distance from O. This is due to the fact that the further the BS is from the user, the further away the center of an obstacle footprint segment needs to be to avoid a blockage.

Consider Assumption 2.3 and the set of points where the segment connecting O with BS i intersects the symmetry axis of each obstacle lane. We approximate $p_{i,{\rm L}}$ with the probability $p_{\rm L}$ that no blockages are present within a distance of $\tau/2$ on either side of the ray connecting the user to BS i. Hence, our approximation is independent on the distance of BS i to O. In particular, $p_{\rm L}$ can be expressed as follows:

$$p_{\rm L} \cong \prod_{\ell=1}^{N_o} e^{-\lambda_{{\rm o},\ell}\tau}, \tag{1}$$

while $p_{i,{\rm N}}$ is approximated as $p_{\rm N} = 1 - p_{\rm L}$. We observe also that the term $e^{-\lambda_{{\rm O},\ell}\tau}$ is the void probability of a one-dimensional PPP of density $\lambda_{{\rm o},\ell}$ [40].

Using the approximation in (1) and invoking the independent thinning theorem of PPP, it follows that the PPP of the LOS BSs $\Phi_{\rm L} \subseteq \Phi_{\rm BS}$ and of the NLOS BS $\Phi_{\rm N} \subseteq \Phi_{\rm BS}$ are independent and with density $\lambda_{\rm L} = p_{\rm L}\lambda_{\rm BS}$ and $\lambda_{\rm N} = p_{\rm N}\lambda_{\rm BS}$, respectively. In addition, the relation $\Phi_{\rm L} \cap \Phi_{\rm N} = \emptyset$ holds.

Consider the i-th BS at a distance $r_i = \sqrt{x_i^2 + y_i^2}$ from the standard user. The indicator function $\mathbf{1}_{i,{\rm L}}$ is equal to one if BS i is in LOS with respect to the standard user, and zero otherwise. The path loss component $\ell(r_i)$ impairing the signal transmitted by BS i and received by the standard user can be defined as follows:

$$\ell(r_i) = \mathbf{1}_{i,{\rm L}} C_{\rm L} r_i^{-\alpha_{\rm L}} + (1-\mathbf{1}_{i,{\rm L}}) C_{\rm N} r_i^{-\alpha_{\rm N}} \tag{2}$$

where $\alpha_{\rm L}$ and $\alpha_{\rm N}$ are the path loss exponents, while $C_{\rm L}$ and $C_{\rm N}$ are the path loss intercept factors in the LOS and NLOS cases, respectively. From Assumption 2.1, we remark that relation $r_i \geq w(N_o+1)$ holds. Hence, for typical values of road lane widths, path loss intercept factors and exponents, relation $w(N_o+1) \geq \max\{C_{\rm L}^{\frac{1}{\alpha_{\rm L}}}, C_{\rm N}^{\frac{1}{\alpha_{\rm N}}}\}$ holds as well[2]. This ensures that both $C_{\rm L} r_i^{-\alpha_{\rm L}}$ and $C_{\rm N} r_i^{-\alpha_{\rm N}}$ are less than or equal to 1.

Assumption 2.4 (BS-Standard User Association): In our system model, the standard user always connects to the BS with index i^*, which is characterized by the minimum path loss component, i.e., $i^* = \arg\max_{i=1,\ldots,b} \{\ell(r_i)\}$.

We assume that the standard user connects to a NLOS BS at a distance r. Since $w(N_o+1) \geq \max\{C_{\rm L}^{\frac{1}{\alpha_{\rm L}}}, C_{\rm N}^{\frac{1}{\alpha_{\rm N}}}\}$, it follows that there are no LOS BSs at a distance smaller than or equal to $A_{\rm L}(r)$, defined as:

$$A_{\rm L}(r) = \max\left\{ w(N_o+1), \left[\frac{C_{\rm N}}{C_{\rm L}} r^{-\alpha_{\rm N}}\right]^{-\frac{1}{\alpha_{\rm L}}} \right\}. \tag{3}$$

We observe that $A_{\rm L}(r)$ is the distance from O for which the path loss component associated with a LOS BS is equal to the path loss component associated with a NLOS BS at a distance r. In a similar way, we observe that if the standard user connects to a LOS BS at a distance r from O, that implies that there are no NLOS BSs at a distance smaller than or equal to $A_{\rm N}(r)$, defined as:

$$A_{\rm N}(r) = \max\left\{ w(N_o+1), \left[\frac{C_{\rm L}}{C_{\rm N}} r^{-\alpha_{\rm L}}\right]^{-\frac{1}{\alpha_{\rm N}}} \right\}. \tag{4}$$

We observe that definitions (3) and (4) avoids $A_{\rm L}(r)$ and $A_{\rm N}(r)$ to be smaller than the distance $w(N_o+1)$ between O and a side of the road, which is clearly not possible.

[2]For instance, we observe that the relation holds for any path loss exponent if $C_{\rm L}=1$, $C_{\rm N}=1$ and $w(N_0+1) \geq 1\,{\rm m}$.

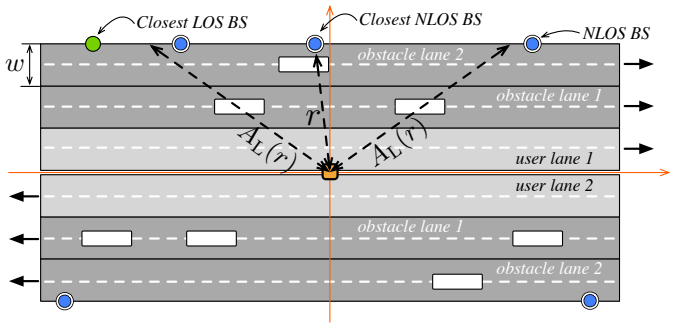

Fig. 2. Proposed BS-standard user association model. In this case, the standard user connects to a NLOS BS.

The standard user will always connect to one BS at a time, which is either the closest LOS or the closest NLOS BS. This choice is made by the standard user according to Assumption 2.4. For instance, Fig. 2 shows the case where the closest LOS BS is at a distance greater than $\mathrm{A_L}(r)$. In this case, the BS associated with the smallest path loss component is the closest NLOS BS, which is at a distance r to the standard user. Those facts allow us to prove the following lemma.

Lemma 2.1: Let $\mathrm{d_L}$ and $\mathrm{d_N}$ be the random variables expressing the distance to the closest LOS and NLOS BSs from the perspective of the standard user, respectively. The Probability Density Function (PDF) of $\mathrm{d_L}$ can be expressed as:

$$f_{\mathrm{L}}(r) = \frac{2\lambda_{\mathrm{L}} r}{b(r)} e^{-2\lambda_{\mathrm{L}} b(r)}, \tag{5}$$

while the PDF of $\mathrm{d_N}$ can be expressed as

$$f_{\mathrm{N}}(r) = \frac{2\lambda_{\mathrm{N}} r}{b(r)} e^{-2\lambda_{\mathrm{N}} b(r)}, \tag{6}$$

where $b(r) = \sqrt{r^2 - w^2(N_o+1)^2}$.

Proof: Considering the LOS case, the proof directly follows from the expression of the PDF of the distance of the closest point to the origin of the axis in a one-dimensional PPP with density λ_{L}, which is $f_{\mathrm{L}}(t) = 2\lambda_{\mathrm{L}} e^{-2\lambda_{\mathrm{L}} t}$ [40, Eq. (2.12)]. By applying the change of variable $t \leftarrow b(r)$ we obtain (5). With similar reasoning, it is also possible to prove (6). ■

From Lemma 2.1, (3) and (4), we prove the following lemma.

Lemma 2.2: The standard user connects to a NLOS BS with probability

$$\mathrm{P_N} = \int_{w(N_o+1)}^{\infty} f_{\mathrm{N}}(r) e^{-2\lambda_{\mathrm{L}} b(A_{\mathrm{L}}(r))}\, dr. \tag{7}$$

On the other hand, the standard user connects to a LOS BS with probability

$$\mathrm{P_L} = \int_{w(N_o+1)}^{\infty} f_{\mathrm{L}}(r) e^{-2\lambda_{\mathrm{N}} b(A_{\mathrm{N}}(r))}\, dr = 1 - \mathrm{P_N}. \tag{8}$$

Proof: Consider the event that the standard user connects to a NLOS BS, which is at a distance r from O. This event is equivalent to that of having all the LOS BSs at a distance greater than or equal to $A_{\mathrm{L}}(r)$. From (5), it follows that $\mathbb{P}[\mathrm{d_L} \geq A_{\mathrm{L}}(r) \text{ and } \mathrm{d_N} = r]$ is equal to $e^{-2\lambda_{\mathrm{L}} b(A_{\mathrm{L}}(r))}$. Then if we marginalize $\mathbb{P}[\mathrm{d_L} \geq A_{\mathrm{L}}(r) \text{ and } \mathrm{d_N} = r]$ with respect to r, we obtain (7). The same reasoning applies to the proof of (8). ■

The gain of the signal received by the standard user depends on the antenna pattern and beam steering performed by each BS and the user. In general, each BS and the standard user are equipped with antenna arrays capable of performing directional beamforming. To capture this feature, we follow [27] and use a sectored approximation to the array pattern. We detail the sectored approximation for our highway model in the following assumption.

Assumption 2.5 (Antenna Pattern): We assume a sectorized model of each BS antenna pattern. In particular, the antenna pattern consists of a main lobe with beamwidth ψ and a side lobe that covers the remainder of the antenna pattern. We assume that the gain of the main lobe is G_{TX} and the gain of the sidelobe is g_{TX}. Similarly, the antenna pattern of the standard user also consists of main lobe with beamwidth ψ and gain G_{RX}, and a side lobe with gain g_{RX}.

The antenna of each BS and the user can be steered. We specify our assumptions for beam steering for BSs and standard user in the following two assumptions.

Assumption 2.6 (BS Beam Steering): Let ϵ_i be the angle between the upper (bottom) side of the road and the antenna boresight of BS i (see Fig. 1). We assume that ϵ_i takes values in $\mathcal{G} = [\frac{\psi}{2}, 2\pi - \frac{\psi}{2}]$. As such, the main lobe of each BS is always entirely directed towards the road portion constrained by the upper and bottom side. If the standard user connects to BS i, the BS steers its antenna beam towards the standard user. On the other hand, if the standard user is not connected to BS i, we assume that ϵ_i takes a value that is uniformly distributed in $\mathcal{G}$.

Assumption 2.7 (Standard User Beam Steering): The angle $\epsilon^{(U)}$ between the positive x-axis and the boresight of the user beam is selected to maximize the gain of the received signal from the serving BS. We assume that $\epsilon^{(U)} \in [\frac{\psi}{2}, \pi - \frac{\psi}{2}]$ or $\epsilon^{(U)} \in [\pi + \frac{\psi}{2}, 2\pi - \frac{\psi}{2}]$ if the user is served by a BS on the upper side or the bottom side of the road respectively. This assumption ensures that interference BSs on the opposite side of the road from the serving BS are always received by a sidelobe, with gain g_{RX}. We also assume that the standard user directs its antenna beam towards the serving BS, which is then received with gain G_{RX}.

III. SINR Outage and Rate Coverage Characterization

For the sake of simplifying the notation and without loss of generality, we say that the BS with index 1 is the BS that the standard user is connected to, while BS $2, \ldots, b$ define the set of the interfering BSs. We define the SINR at the location of the standard user as follows:

$$\mathrm{SINR}_O = \frac{|h_1|^2\, \Delta_1\, \ell(r_1)}{\sigma + \mathrm{I}}, \tag{9}$$

where

$$\mathrm{I} = \sum_{j=2}^{b} |h_j|^2\, \Delta_j\, \ell(r_j). \tag{10}$$

Terms h_i and Δ_i are the small-scale fading component and the overall transmit/receive antenna gain associated with BS i transmissions, respectively, for $i = 1, \ldots, b$. Term I is the total interference contribution determined by all the BSs except the one connected to the standard user, i.e., the total interference determined by BS $2, \ldots, b$. From Assumption 2.6 and 2.7, it follows that Δ_1 is equal to $G_{\mathrm{TX}}G_{\mathrm{RX}}$. Finally, σ represents the thermal noise power normalized with respect to the transmission power P_t.

As acknowledged in [9] there is a lack of extensive measurements for vehicular mmWave networks, as well as widely accepted channel models. However, we observe that [41]: (i) because of the beamforming capabilities and the sectorial antenna pattern, the signal is impaired only by a limited number of scatterers, and (ii) the interfering transmissions cluster with many scatterers and reach the standard user. We observe that the considered sectorial antennal model at the transmitter and receiver sides (see Assumption 2.5) significantly reduces the angular spread of the incoming signals - thus reducing the Doppler spread. Furthermore, the incoming signals are concentrated in one direction. Hence, it is likely to observe a non-zero bias in the Doppler spectrum, which can be compensated by the automatic frequency control loop at the receiver side [42]. For these reasons, the Doppler effect has not been considered.

Assumption 3.1 (Channel Model): The channel between the serving BS and standard user is described by a Nakagami channel model with parameter m, and hence, $|h_1|^2$ follows a gamma distribution (with shape parameter m and rate equal to 1). On the other hand, the channels between the standard user and each interfering BS are modelled as independent Rayleigh channels - thus $|h_2|^2, \ldots, |h_b|^2$ are independently and identically distributed as an exponential distribution with mean equal to 1.

TABLE III
VALUES OF (a, b, Δ) FOR DIFFERENT $< |\mathrm{x}_1|, \mathbb{S}_1, \mathbb{E}_1, \mathrm{S}, \mathrm{E} >$.

Configuration of $< \mathbb{S}_1, \mathbb{E}_1, \mathrm{S}, \mathrm{E} >$	**Conditions on** $\lvert x_1 \rvert$	**Enumeration of elements** $(a, b, \Delta) \in \mathcal{C}_{\lvert \mathrm{x}_1 \rvert, \mathbb{S}_1, \mathbb{E}_1, \mathrm{S}, \mathrm{E}}$
$< \mathrm{U}, \mathrm{L}, \mathrm{U}, \mathrm{L} >$	For any $\lvert x_1 \rvert$ such that $J > 0$	$(\lvert x_1 \rvert, K, g_{\mathrm{TX}}G_{\mathrm{RX}})$, $(K, +\infty, g_{\mathrm{TX}}g_{\mathrm{RX}})$, $(\lvert x_1 \rvert, +\infty, g_{\mathrm{TX}}g_{\mathrm{RX}})$
	For any $\lvert x_1 \rvert$ such that $J \leq 0$	$(\lvert x_1 \rvert, K, g_{\mathrm{TX}}G_{\mathrm{RX}})$, $(K, +\infty, g_{\mathrm{TX}}g_{\mathrm{RX}})$, $(\lvert x_1 \rvert, \lvert J \rvert, g_{\mathrm{TX}}G_{\mathrm{RX}})$, $(\lvert J \rvert, +\infty, g_{\mathrm{TX}}g_{\mathrm{RX}})$
$< \mathrm{U}, \mathrm{L}, \mathrm{U}, \mathrm{N} >$	For any $\lvert x_1 \rvert$ such that $J > 0$	$(x_{\mathrm{N}}(r_1), J, g_{\mathrm{TX}}g_{\mathrm{RX}})$, $(x_{\mathrm{N}}(r_1), +\infty, g_{\mathrm{TX}}g_{\mathrm{RX}})$, $(J, K, g_{\mathrm{TX}}G_{\mathrm{RX}})$, $(K, +\infty, g_{\mathrm{TX}}g_{\mathrm{RX}})$
	For any $\lvert x_1 \rvert$ such that $J \leq 0$	Refer to the case $< \mathrm{U}, \mathrm{L}, \mathrm{U}, \mathrm{L} > (J \leq 0)$ and replace $\lvert x_1 \rvert$ with $x_{\mathrm{N}}(r_1)$
$< \mathrm{U}, \mathrm{L}, \mathrm{B}, \mathrm{L} >$	For any $\lvert x_1 \rvert$	$(\lvert x_1 \rvert, +\infty, g_{\mathrm{TX}}g_{\mathrm{RX}})$, $(\lvert x_1 \rvert, +\infty, g_{\mathrm{TX}}g_{\mathrm{RX}})$,
$< \mathrm{U}, \mathrm{L}, \mathrm{B}, \mathrm{N} >$	Refer to the case $< \mathrm{U}, \mathrm{L}, \mathrm{B}, \mathrm{L} >$ and replace $\lvert x_1 \rvert$ with $x_{\mathrm{N}}(r_1)$	
$< \mathrm{U}, \mathrm{N}, \mathrm{U}, \mathrm{L} >$	For any $\lvert x_1 \rvert$ such that $x_{\mathrm{L}}(r_1) > K$	Refer to the case $< \mathrm{U}, \mathrm{L}, \mathrm{B}, \mathrm{L} >$ and replace $\lvert x_1 \rvert$ with $x_{\mathrm{L}}(r_1)$
	For any $\lvert x_1 \rvert$ such that $x_{\mathrm{L}}(r_1) \leq K$	Refer to the case $< \mathrm{U}, \mathrm{L}, \mathrm{U}, \mathrm{L} >$ and replace $\lvert x_1 \rvert$ with $x_{\mathrm{L}}(r_1)$
$< \mathrm{U}, \mathrm{N}, \mathrm{U}, \mathrm{N} >$	Refer to the case $< \mathrm{U}, \mathrm{L}, \mathrm{U}, \mathrm{L} >$	
$< \mathrm{U}, \mathrm{N}, \mathrm{B}, \mathrm{L} >$	Refer to the case $< \mathrm{U}, \mathrm{L}, \mathrm{B}, \mathrm{L} >$ and replace x_1 with $x_{\mathrm{L}}(r_1)$	
$< \mathrm{U}, \mathrm{N}, \mathrm{B}, \mathrm{N} >$	Refer to the case $< \mathrm{U}, \mathrm{L}, \mathrm{B}, \mathrm{L} >$	
Cases where $\mathbb{S}_1 = \mathrm{B}$, $\mathrm{S} = \mathrm{B}$	Refer to the correspondent cases where $\mathbb{S}_1 = \mathrm{U}$ and $\mathrm{S} = \mathrm{U}$	
Cases where $\mathbb{S}_1 = \mathrm{B}$, $\mathrm{S} = \mathrm{U}$	Refer to the correspondent cases where $\mathbb{S}_1 = \mathrm{U}$ and $\mathrm{S} = \mathrm{B}$	

A. Analytical Characterization of I

In order to provide an analytical characterization of the interference power at O, it is convenient to split the term I into four different components: (i) $\mathrm{I}_{\mathrm{U,L}}$ and $\mathrm{I}_{\mathrm{U,N}}$ representing the interference power associated with LOS and NLOS BSs placed on the upper side of the road whose positions are defined by the PPPs $\Phi_{\mathrm{U,L}}$ and $\Phi_{\mathrm{U,N}}$, respectively, and, (ii) $\mathrm{I}_{\mathrm{B,L}}$ and $\mathrm{I}_{\mathrm{B,N}}$ the interference power generated by LOS and NLOS BSs on the bottom side of the road placed at the location given by the PPPs $\Phi_{\mathrm{B,L}}$ and $\Phi_{\mathrm{B,N}}$. Overall, the total interference power is given by $\mathrm{I} = \sum_{\mathrm{S}\in\{\mathrm{U,B}\},\mathrm{E}\in\{\mathrm{L,N}\}} \mathrm{I}_{\mathrm{S,E}}$. In addition, the relations $\Phi_{\mathrm{L}} = \Phi_{\mathrm{U,L}} \bigcup \Phi_{\mathrm{B,L}}$ and $\Phi_{\mathrm{N}} = \Phi_{\mathrm{U,N}} \bigcup \Phi_{\mathrm{B,N}}$ hold.

In the following result, we derive an approximation of the Laplace transform $\mathcal{L}_{\mathrm{I}}(s)$ of I.

Theorem 3.1: Let $\mathbb{S}_1 = \mathrm{U}$ and $\mathbb{S}_1 = \mathrm{B}$ represent the cases where the standard user connects to a BS on the upper or the bottom side of the road, respectively. In addition, let $\mathbb{E}_1 = \mathrm{L}$ and $\mathbb{E}_1 = \mathrm{N}$ signify the cases where the standard user connects to a LOS or NLOS BS, respectively. The Laplace transform $\mathcal{L}_{\mathrm{I}_{\mathrm{S,E}},\mathbb{E}_1}(s)$ of $\mathrm{I}_{\mathrm{S,E}}$, conditioned on $\mathbb{E}_1$, for $\mathrm{S} \in \{\mathrm{U}, \mathrm{B}\}$ and $\mathrm{E} \in \{\mathrm{L}, \mathrm{N}\}$, can be approximated as follows:

$$\mathcal{L}_{\mathrm{I}_{\mathrm{S,E}},\mathbb{E}_1}(s) \cong \prod_{\substack{\mathbb{S}_1\in\{\mathrm{U,B}\},\\ (a,b,\Delta)\in\mathcal{C}_{|\mathrm{x}_1|,\mathbb{S}_1,\mathbb{E}_1,\mathrm{S,E}}}} \sqrt{\mathcal{L}_{\mathrm{I}_{\mathrm{S,E}},\mathbb{E}_1}(s; a, b, \Delta)}, \qquad (11)$$

where $\mathcal{L}_{\mathrm{I}_{\mathrm{S,E}},\mathbb{E}_1}(s; a, b, \Delta)$ is defined as in (31). We define the x-axis coordinates J and K of the points where the two rays defining the standard user beam intersect with a side of the road, as $J = w(N_o + 1)/[\tan(\epsilon^{(\mathrm{U})} + \psi/2)]$ and $K = w(N_o + 1)/[\tan(\epsilon^{(\mathrm{U})} - \psi/2)]$, where $\epsilon^{(\mathrm{U})} = \tan^{-1}[w(N_o + 1)/x_1]$ (see Fig. 10). Furthermore, let us define $x_{\mathrm{L}}(r_1) = \sqrt{(\mathrm{A}_{\mathrm{L}}(r_1))^2 - w^2(N_o + 1)^2}$ and $x_{\mathrm{N}}(r_1) = \sqrt{(\mathrm{A}_{\mathrm{N}}(r_1))^2 - w^2(N_o + 1)^2}$. Different combinations of parameters $< |\mathrm{x}_1|, \mathbb{S}_1, \mathbb{E}_1, \mathrm{S}, \mathrm{E} >$ determine different sequences $\mathcal{C}_{|\mathrm{x}_1|,\mathbb{S}_1,\mathbb{E}_1,\mathrm{S,E}}$ of parameter configurations (a, b, Δ), as defined in Table III.

Proof: See Appendix A. ■

Example 3.1: Consider the scenario where the standard user connects to a LOS BS, i.e., $\mathbb{E}_1 = \mathrm{L}$, and relation $J > 0$ holds. We evaluate the Laplace transform of the interference associated with the BSs located on the upper sider of the road ($\mathrm{S} = \mathrm{U}$) that are in LOS with respect to the standard user ($\mathrm{E} = \mathrm{L}$). Sequence $\mathcal{C}_{|\mathrm{x}_1|,\mathrm{U,L,U,L}}$ is given by the first row of Table III, while $\mathcal{C}_{|\mathrm{x}_1|,\mathrm{B,L,U,L}}$ consists exactly of the same elements of sequence $\mathcal{C}_{|\mathrm{x}_1|,\mathrm{U,L,B,L}}$ (last row of Table III). As

a result, $\mathcal{L}_{\mathrm{I_{S,E},\mathbb{E}_1}}(s)$ can be approximated as follows:

$$\begin{aligned}\mathcal{L}_{\mathrm{I_{S,E},\mathbb{E}_1}}(s) \cong \Big[&\mathcal{L}_{\mathrm{I_{S,E},\mathbb{E}_1}}(s;|x_1|,K,g_{\mathrm{TX}}G_{\mathrm{RX}})\\ &\cdot\mathcal{L}_{\mathrm{I_{S,E},\mathbb{E}_1}}(s;K,+\infty,g_{\mathrm{TX}}g_{\mathrm{RX}})\\ &\cdot\mathcal{L}_{\mathrm{I_{S,E},\mathbb{E}_1}}(s;|x_1|,+\infty,g_{\mathrm{TX}}g_{\mathrm{RX}})\Big]^{1/2}\\ &\cdot\mathcal{L}_{\mathrm{I_{S,E},\mathbb{E}_1}}(s;x_{\mathrm{N}}(r_1),+\infty,g_{\mathrm{TX}}g_{\mathrm{RX}}). \quad (12)\end{aligned}$$

From Theorem 3.1 and from the fact that I is defined as a sum of statistically independent interference components, it possible to prove the following corollary.

Corollary 3.1: The Laplace transform of I, for $\mathbb{E}_1 = \{\mathrm{L},\mathrm{N}\}$, can be approximated as follows:

$$\mathcal{L}_{\mathrm{I},\mathbb{E}_1}(s) \cong \prod_{\mathrm{S}\in\{\mathrm{U},\mathrm{B}\},\mathrm{E}\in\{\mathrm{L},\mathrm{N}\}} \mathcal{L}_{I_{\mathrm{S,E}},\mathbb{E}_1}(s) \quad (13)$$

Example 3.2: Consider the scenario where $\mathbb{E}_1 = \mathrm{L}$, and relation $J > 0$ holds. By resorting to Corollary 3.1, $\mathcal{L}_{\mathrm{I_{S,E},\mathbb{E}_1}}(s)$ can be approximated as follows:

$$\begin{aligned}\mathcal{L}_{\mathrm{I},\mathbb{E}_1}(s) \cong\ &\mathcal{L}_{\mathrm{I_{S,E},\mathbb{E}_1}}(s;|x_1|,K,g_{\mathrm{TX}}G_{\mathrm{RX}})\\ &\cdot\mathcal{L}_{\mathrm{I_{S,E},\mathbb{E}_1}}(s;x_{\mathrm{N}}(r_1),J,g_{\mathrm{TX}}g_{\mathrm{RX}})\\ &\cdot\mathcal{L}_{\mathrm{I_{S,E},\mathbb{E}_1}}(s;J,K,g_{\mathrm{TX}}G_{\mathrm{RX}})\\ &\cdot\left(\mathcal{L}_{\mathrm{I_{S,E},\mathbb{E}_1}}(s;K,+\infty,g_{\mathrm{TX}}g_{\mathrm{RX}})\right)^2\\ &\cdot\left(\mathcal{L}_{\mathrm{I_{S,E},\mathbb{E}_1}}(s;|x_1|,+\infty,g_{\mathrm{TX}}g_{\mathrm{RX}})\right)^3\\ &\cdot\left(\mathcal{L}_{\mathrm{I_{S,E},\mathbb{E}_1}}(s;x_{\mathrm{N}}(r_1),+\infty,g_{\mathrm{TX}}g_{\mathrm{RX}})\right)^3 \quad (14)\end{aligned}$$

B. SINR Outage and Rate Coverage Probability Framework

The general framework for evaluating the SINR outage probability is given in the following result.

Theorem 3.2: Let us signify with

$$\mathrm{F_L}(t) = e^{-2\lambda_{\mathrm{L}}\sqrt{t^2-w^2(N_o+1)^2}} \quad (15)$$

and

$$\mathrm{F_N}(t) = e^{-2\lambda_{\mathrm{N}}\sqrt{t^2-w^2(N_o+1)^2}} \quad (16)$$

the probability of a LOS or NLOS BS not being at a distance smaller than t from O, respectively. We regards $\mathrm{P_T}(\theta)$ to be the SINR outage probability with respect to a threshold θ, i.e., the probability that SINR_O is smaller than a threshold θ, $\mathrm{P_T}(\theta)$ can be expressed as follows:

$$\begin{aligned}\mathrm{P_T}(\theta) = \mathrm{P_L} - \overbrace{\mathbb{P}[\mathrm{SINR}_O > \theta \wedge \text{std. user served in LOS}]}^{\mathrm{P_{CL}}(\theta)}\\ + \mathrm{P_N} - \underbrace{\mathbb{P}[\mathrm{SINR}_O > \theta \wedge \text{std. user served in NLOS}]}_{\mathrm{P_{CN}}(\theta)} \quad (17)\end{aligned}$$

where

$$\begin{aligned}\mathrm{P_{CL}}(\theta) =& \Big|_{\mathbb{E}_1=\mathrm{L}} - \sum_{k=0}^{m-1}(-1)^{m-k}\binom{m}{k}\int_{w(N_o+1)}^{+\infty} e^{-\frac{v\sigma\theta(m-k)}{\Delta_1\mathrm{C_L}}r_1^{\alpha_{\mathrm{L}}}}\\ &\cdot\mathcal{L}_{\mathrm{I},\mathbb{E}_1}\left(\frac{v\theta r_1^{\alpha_{\mathrm{L}}}(m-k)}{\Delta_1\mathrm{C_L}}\right) f_{\mathrm{L}}(r_1)\mathrm{F_N}(\mathrm{A_N}(r_1))\,dr_1 \quad (18)\end{aligned}$$

and

$$\begin{aligned}\mathrm{P_{CN}}(\theta) =& \Big|_{\mathbb{E}_1=\mathrm{N}} - \sum_{k=0}^{m-1}(-1)^{m-k}\binom{m}{k}\int_{w(N_o+1)}^{+\infty} e^{-\frac{v\sigma\theta(m-k)}{\Delta_1\mathrm{C_N}}r_1^{\alpha_{\mathrm{N}}}}\\ &\cdot\mathcal{L}_{\mathrm{I},\mathbb{E}_1}\left(\frac{v\theta r_1^{\alpha_{\mathrm{N}}}(m-k)}{\Delta_1\mathrm{C_N}}\right) f_{\mathrm{N}}(r_1)\mathrm{F_L}(\mathrm{A_L}(r_1))\,dr_1, \quad (19)\end{aligned}$$

represent the probability of the standard user not experiencing SINR outage while connected to a LOS or NLOS BS, respectively.

Proof: Considering (17), the overall expression is straightforward. Hence, we limit to show how $\mathrm{P_{CL}}(\theta)$ and $\mathrm{P_{CN}}(\theta)$ have been derived. In particular, the following relation holds (for $\mathbb{E}_1 = \mathrm{L}$):

$$\begin{aligned}\mathrm{P_{CL}}(\theta) &= \mathbb{P}\left[\frac{|h_1|^2\,\Delta_1\,\ell(r_1)}{\sigma+\mathrm{I}} > \theta \wedge \text{std. user served in LOS}\right]\\ &\overset{(i)}{\cong} \mathbb{E}_{\mathrm{I}}\int_{w(N_o+1)}^{+\infty}\left(1-\left(1-e^{-v\frac{(\sigma+\mathrm{I})\theta}{\Delta_1\mathrm{C_L}}r_1^{\alpha_{\mathrm{L}}}}\right)^m\right)\\ &\quad\cdot f_{\mathrm{L}}(r_1)\mathrm{F_N}(\mathrm{A_N}(r_1))\,dr_1 \quad (20)\end{aligned}$$

where $v = m(m!)^{-1/m}$ [27, Lemma 6] and (i) arise from $|h_1|^2$ being distributed as a gamma random variable. In addition, $\mathrm{F_N}(\mathrm{A_N}(r_1))$ is defined as the probability of a NLOS BS not being at a distance smaller than $\mathrm{A_N}(r_1)$ to O, i.e., the probability that the standard user is not connected to a NLOS BS. The expression of $\mathrm{F_N}(t)$, as in (16), immediately follows from the simplification of the following:

$$\mathrm{F_N}(t) = 1 - \int_{w(N_o+1)}^{t} f_{\mathrm{N}}(r)\,dr. \quad (21)$$

From the binomial theorem, bringing inside of the integral sign the expectation with respect to I and invoking Corollary 3.1 we obtain (18). By following the same reasoning, it is also possible to derive expressions for $\mathrm{P_{CN}}(\theta)$ and $\mathrm{F_L}(t)$. ■

As the value of α_{N} increases it is less likely that the standard user connects to a NLOS BS. This intuition can be readily confirmed from (17) as follows.

Remark 3.1: From (4), A_{N} is likely to be equal to $w(N_o+1)$, for large values of α_{N}. As a result, the exponential term in (8) approaches one and, hence, $\mathrm{P_L}$ can be approximated as follows:

$$\mathrm{P_L} \cong \int_{w(N_o+1)}^{\infty} f_{\mathrm{L}}(r)\,dr = \int_0^{\infty} 2\lambda_{\mathrm{L}}e^{-2\lambda_{\mathrm{L}}t} = 1. \quad (22)$$

Using this approximation, it follows that $\mathrm{P_N} \cong 0$ holds. In addition, since $\mathrm{P_{CN}}$ is always less than or equal to $\mathrm{P_N}$, the relation $\mathrm{P_{CN}} \cong 0$ holds as well. If $A_{\mathrm{N}} \cong w(N_o+1)$, the relation $\mathrm{F_N}(\mathrm{A_N}(r_1)) \cong 1$ holds. For these reasons, $\mathrm{P_T}(\theta)$ can be approximated as follows:

$$\begin{aligned}\mathrm{P_T}(\theta) \cong 1 + &\sum_{k=0}^{m-1}(-1)^{m-k}\binom{m}{k}\int_{w(N_o+1)}^{+\infty} e^{-\frac{v\sigma\theta(m-k)}{\Delta_1\mathrm{C_L}}r_1^{\alpha_{\mathrm{L}}}}\\ &\cdot\mathcal{L}_{\mathrm{I},\mathbb{E}_1}\left(\frac{v\theta r_1^{\alpha_{\mathrm{L}}}(m-k)}{\Delta_1\mathrm{C_L}}\right) f_{\mathrm{L}}(r_1)\,dr_1. \quad (23)\end{aligned}$$

From [35, Theorem 1] and by using Theorem 3.2, it is now possible to express the rate coverage probability $\mathrm{R_C}(\kappa)$, i.e.,

TABLE IV
MAIN SIMULATION PARAMETERS.

Parameter	Value
Length of the simulated road section (i.e., $2R$)	$20\,\mathrm{km}$, $100\,\mathrm{km}$
w	$3.7\,\mathrm{m}$, as per [43]
Position of the standard user	$(0,0)$, $(0,-w/2)$
τ	$11.1\,\mathrm{m}$, as per [44]
N_o	1,2
$\{\lambda_{o,1},\lambda_{o,2}\}$	$\{1\cdot10^{-2},2\cdot10^{-2}\}$, i.e., one blockage every $\{100\,\mathrm{m},50\,\mathrm{m}\}$
λ_{BS}	from $2\cdot10^{-4}$ to $1\cdot10^{-2}$, with a step of $2\cdot10^{-4}$
$\mathrm{C_L}$, $\mathrm{C_N}$	1
α_{L}	2.8
α_{N}	3.86
m	3, as per [41]
ϕ	$\{30^{\circ},90^{\circ}\}$
G_{TX}	$\{10\,\mathrm{dB},20\,\mathrm{dB}\}$
G_{RX}	$10\,\mathrm{dB}$
g_{TX}, g_{RX}	$-10\,\mathrm{dB}$
W	$100\,\mathrm{MHz}$
P_t	$27\,\mathrm{dBm}$
Thermal noise power (i.e, $\sigma\cdot P_t$)	$10\log_{10}(k\cdot T\cdot W\cdot10^3)$ dBm, where k is the Boltzmann constant and the temperature $T=290\,\mathrm{K}$ [19]

the probability that the standard user experiences a rate that is greater than or equal to κ. In particular, the rate coverage probability is given by:

$$\begin{aligned}\mathrm{R_C}(\kappa)&=\mathbb{P}[\text{rate of std. user}\geq\kappa]\\&=1-\mathrm{P_T}(2^{\kappa/W}-1),\end{aligned}\tag{24}$$

where W is the system bandwidth.

IV. Numerical Results

A. Simulation Framework

In order to numerically study our mmWave highway network and validate the proposed theoretical model, we developed a Monte Carlo simulation framework for characterizing both the SINR outage probability $\mathrm{P_T}$ and the rate coverage probability $\mathrm{R_C}$. As such, the simulator estimates $\mathrm{P_T}$ and $\mathrm{R_C}$ by averaging over a large number of iterations. In particular, during each simulation iteration, a new network scenario is randomly generated. In each scenario, the assumptions provided in Sections II and III hold. For instance, BSs are positioned according to an instance of the random process as in Assumption 2.2. The same applies to the positioning of the obstacles, the steering angle of the interfering BSs, etc. Both our computer simulator and the implementation of the proposed theoretical framework are available online[3] from [45].

We remark that Assumption 2.1 assumes that the highway is infinitely long, which is not possible in a simulation. However, as noted in [46], [47], the radius R of the simulated system can be related to the simulation accuracy error ε, as in [46, Eq. (3.5)]. In the case of a one-dimensional PPP, the radius is related to the simulation error by $R\geq\varepsilon^{-\frac{1}{\alpha_{\mathrm{L}}-1}}$.

With regards to Table IV, we refer to $N_o=\{1,2\}$ obstacle lanes per driving direction. For $N_o=2$, we assumed different traffic intensities by setting densities $\{\lambda_{o,1},\lambda_{o,2}\}$ as per row six of Table IV. We set the footprint segment length τ equal to the maximum length of a double-decker bus [44]. Furthermore, we consider a typical highway lane width w [43].

In order to effectively validate the proposed BS-standard user association paradigm, we avoided scenarios where it was unlikely for the the standard user to connect to a NLOS BS (see Remark 3.1), such as $\alpha_{\mathrm{N}}\geq5.76$. To this end, we set the path loss exponents $\alpha_{\mathrm{L}}=2.8$ and $\alpha_{\mathrm{N}}=3.86$, which are realistic values for mmWave links [18]. In Section II-A, we approximated the probabilities p_{L} and p_{N} for a BS being in LOS or NLOS with respect to O, respectively. It is worth noting that the approximation in (1) has been invoked only in the derivation of the proposed theoretical model. In contrast, the simulated scenarios whether a BS is in LOS or NLOS is determined only by the conditions in Assumption 2.3. As such, a BS is in NLOS only if the direct ray connecting the standard user and the BS is blocked by one or more footprint segments (see Section II-A). Finally, we remark that the standard user connects to the BS characterized by the smallest path loss component (see Assumption 2.7). In our simulations this is made possible by assuming that the standard user has perfect channel state information. All the remaining simulation parameters are summarized in Table IV.

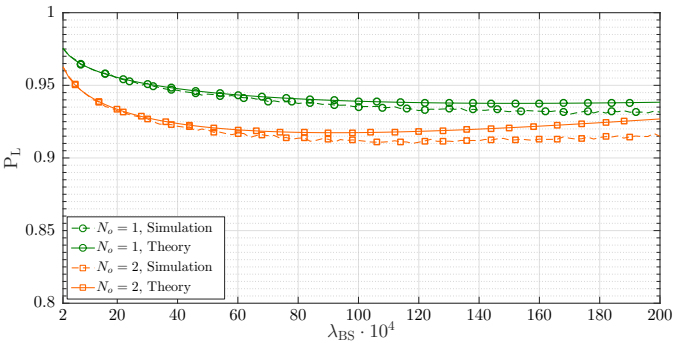

Fig. 3. Probability $\mathrm{P_L}$ that the standard users connects to a LOS BS as a function of λ_{BS}, for $N_o=1$ and 2.

B. Theoretical Model Assessment and Network Performance Investigation

In order to numerically study our mmWave highway network and assess the accuracy of our theoretical model, we firstly refer to a scenario where the standard user is located at O. In addition, we refer to a road section with a length $R=100\,\mathrm{km}$, which ensures a value of $\varepsilon\geq10^{-7.2}$, when $\alpha_{\mathrm{L}}=2.8$.

Considering the density λ_{BS} of process Φ_{BS}, we ideally project the BSs onto the x-axis and we define their projected mean Inter-Site-Distance (x-ISD) as $1/\lambda_{\mathrm{BS}}$.

Fig. 3 shows the probability of the standard user connecting to a LOS BS as a function of λ_{BS} for one and two obstacle lanes on each side of the road. From Lemma 2.2, it follows that the value of $\mathrm{P_L}$ and, hence, of $\mathrm{P_N}$ depends only on λ_{BS}, the footprint segment, the densities of the obstacle processes, the layout of the road and the path loss exponent. We also observe that the equivalent x-ISD spans between $5\,\mathrm{km}$ ($\lambda_{\mathrm{BS}}=2\cdot10^{-4}$)

[3]The whole software package will be made publicly available at the moment of the publication of this manuscript.

and $50\,\mathrm{m}$ ($\lambda_{\mathrm{BS}} = 2 \cdot 10^{-2}$). In particular, as typically happens, we observe that $\mathrm{P_L}$ is significantly greater than $\mathrm{P_N}$; however, $\mathrm{P_N}$ is not negligible. In fact, if $N_o = 1$ then, for $\lambda_{\mathrm{BS}} = 4{\cdot}10^{-3}$ ($\lambda_{\mathrm{BS}} = 10^{-2}$), $\mathrm{P_L}$ is equal to 0.95 (0.93). When N_o increases to 2, the value of $\mathrm{P_L}$ drops to 0.92 and 0.91, for $\lambda_{\mathrm{BS}} = 4{\cdot}10^{-3}$ and $\lambda_{\mathrm{BS}} = 10^{-2}$, respectively.

Fig. 3 also compares our approximated theoretical expression of $\mathrm{P_L}$, as in (8), with the simulated one. We note that (8) underestimates $\mathrm{P_L}$, and, hence, (7) overestimates $\mathrm{P_N}$. However, we observe that: (i) for $\lambda_{\mathrm{BS}} \in [2 \cdot 10^{-4}, 10^{-2}]$, the underestimation error is negligible (it is smaller than $6.5{\cdot}10^{-3}$), and (ii) for dense scenarios ($\lambda_{\mathrm{BS}} > 10^{-2}$), it never exceeds $1.3{\cdot}10^{-2}$. Overall, the maximum Mean Squared Error (MSE) between simulation and theory is $4{\cdot}10^{-5}$. From Fig. 3, we also conclude that $\mathrm{P_L}$ may have a non-trivial minimum. In our scenarios, this is particularly evident when $N_o = 2$.

Remark 4.1: As we move from sparse to dense scenarios, it becomes more likely for a NLOS BS to be closer to the standard user; thus $\mathrm{P_L}$ decreases. However, this reasoning holds up to a certain value of density. In fact, at some point, the BS density becomes so high that it becomes increasingly unlikely not to have a LOS BS that is close enough to serve the standard user. This phenomenon may generate a non-trivial minimum in $\mathrm{P_L}$.

We note that the behavior pointed out in the previous remark is also captured by the proposed theoretical model. For these reasons, we can conclude that (7) and (8) are a good approximation to the probabilities $\mathrm{P_N}$ and $\mathrm{P_L}$.

Fig. 4 shows the effect of the SINR threshold θ on the outage probability $\mathrm{P_T}(\theta)$, for $N_o = 1$, several antenna beamwidth ψ values and a range of BS transmit antenna gains G_{TX}. Here, the vehicular receive antenna gain is set to $G_{\mathrm{RX}} = 10\,\mathrm{dB}$.

In Fig. 4a, the x-ISD is fixed at $100\,\mathrm{m}$. It should be noted that the proposed theoretical model, as in Theorem 3.2, not only follows the trend of the simulated values of $\mathrm{P_T}(\theta)$ but also it is a tight upper-bound for our simulations for the majority of the values of θ. In addition, the deviation between theory and simulation is negligible when $\theta \in [-5\,\mathrm{dB}, 15\,\mathrm{dB}]$ or $\theta \in [-5\,\mathrm{dB}, 10\,\mathrm{dB}]$, for $G_{\mathrm{TX}} = 10\,\mathrm{dB}$ or $G_{\mathrm{TX}} = 20\,\mathrm{dB}$, respectively. On the other hand, that deviation gradually increases as θ becomes larger. Nevertheless, the maximum MSE between simulation and theory is smaller than $4.1 \cdot 10^{-3}$. Overall, we observe the following facts:

- Changing the beamwidth from $30°$ to $90°$ alters the SINR outage probability by a maximum of $5.6 \cdot 10^{-2}$. This can be intuitively explained by noting that the serving BS is likely to be close to the vertical symmetry axis of our system model. From Assumption 2.7, the standard user aligns its beam towards the serving BS. As such, the values of J and K (see Theorem 3.1) do not largely change on passing from $\psi = 30°$ to $\psi = 90°$. Thus, for the interference component to become substantial, the value of ψ should be quite large.
- Overall, we observe that when the beamwidth increases, $\mathrm{P_T}$ increases as well. Intuitively, that is because the standard user is likely to receive a large interference contribution via the main antenna lobe, for larger values of ψ.

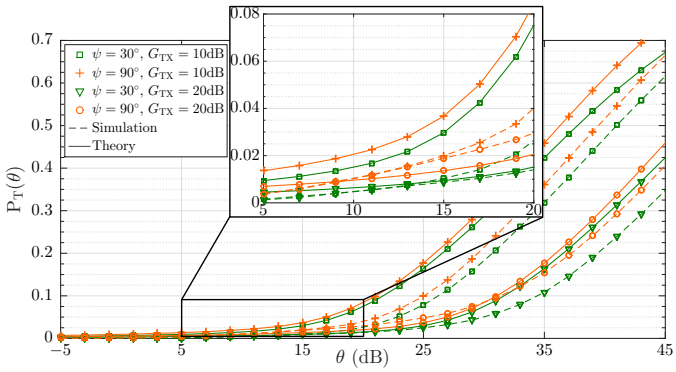

(a) $\lambda_{\mathrm{BS}} = 10^{-2}$, x-ISD = 100 m

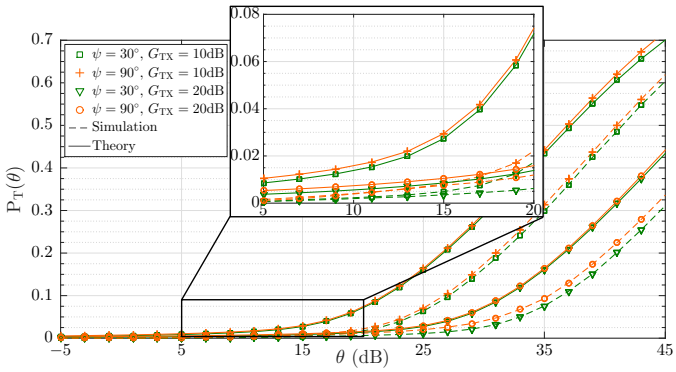

(b) $\lambda_{\mathrm{BS}} = 4 \cdot 10^{-3}$, x-ISD = 250 m

Fig. 4. SINR outage probability $\mathrm{P_T}$ as a function of the threshold θ, for $N_o = 1$, $\psi = \{30°, 90°\}$ and $G_{\mathrm{TX}} = \{10\,\mathrm{dB}, 20\,\mathrm{dB}\}$.

- Increasing the value of the maximum transmit antenna gain (from $10\,\mathrm{dB}$ to $20\,\mathrm{dB}$) results in a reduction of the SINR outage probability that, for large values of θ, can be greater than 0.25. This clearly suggests that the increment on the interfering power is always smaller than or equal to the correspondent increment on the signal power. This is mainly because of the directivity of the considered antenna model.

Fig. 4b refers to the same scenarios as in Fig. 4a except for the x-ISD that is equal to $250\,\mathrm{m}$. In general, we observe that the comments to Fig. 4a still hold. In particular, we observe that this time the proposed theoretical model proves to be a tight upper-bound for the simulated values (the MSE is $6.7 \cdot 10^{-3}$). Furthermore, the impact of the value of ψ on $\mathrm{P_T}$ becomes negligible. Intuitively, this can be explained by noting that the number of interfering BSs that are going to be received by the standard user with the maximum antenna gain decreases as λ_{BS} decreases. However, as the BS density decreases (the BSs are more sparsely deployed), it becomes more likely (up a certain extent) that the number of interfering BSs remains the same, even for a beamwidth equal to $90°$.

Fig. 5 refers to the same scenarios as Fig. 4 but this time we consider two obstacle lanes on each side of the road ($N_o = 2$). In addition to the discussion for Fig. 4, we note the following:

- For the smallest value of the antenna transmit gain ($G_{\mathrm{TX}} = 10\,\mathrm{dB}$), both the simulated and the proposed theoretical model produce values of $\mathrm{P_T}$ that are negligibly greater that those when $N_o = 1$.

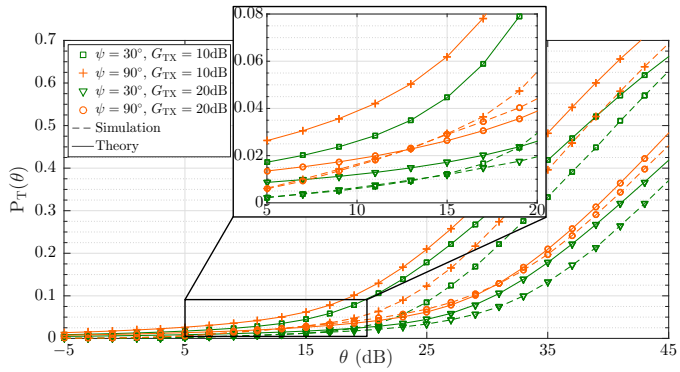

(a) $\lambda_{BS} = 10^{-2}$, x-ISD = 100 m

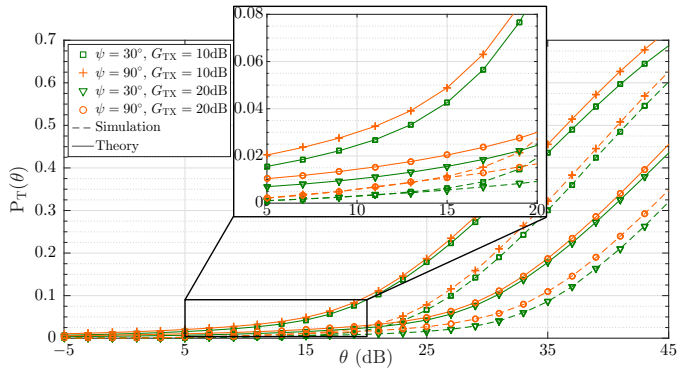

(b) $\lambda_{BS} = 4 \cdot 10^{-3}$, x-ISD = 250 m

Fig. 5. SINR outage probability P_T as a function of the threshold θ, for $N_o = 2$, $\psi = \{30°, 90°\}$ and $G_{TX} = \{10\,\text{dB}, 20\,\text{dB}\}$.

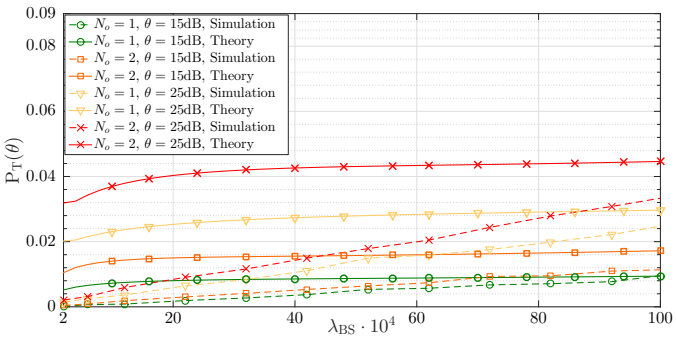

Fig. 6. SINR outage probability P_T as a function of the BS density λ_{BS}, for $\theta = \{15\,\text{dB}, 25\,\text{dB}\}$ dB, $N_o = \{1, 2\}$, $\psi = 30°$ and $G_{TX} = 20\,\text{dB}$.

- For x-ISD = 100 m and $G_{TX} = 20\,\text{dB}$, the SINR outage is slightly greater that the correspondent case as in Fig. 4a. In particular, for $\theta \geq 21\,\text{dB}$, we observe an increment in the simulated values of P_T of more than 10^{-2}.
- As soon as we refer to a sparser network scenario, x-ISD = 250 m, the conclusions drawn for Fig. 4b also apply for Fig. 5b. Hence, the impact of ψ on P_T vanishes.

In Fig. 4 and Fig. 5, we already observed that the proposed theoretical model, as in Theorem 3.2, follows well the trend of the corresponding simulated values, and it is characterized by an error that is negligible for most important values of θ (e.g., $\theta \leq 25\,\text{dB}$). These facts are further confirmed by Fig. 6, which shows the value of P_T as as a function of λ_{BS}, for

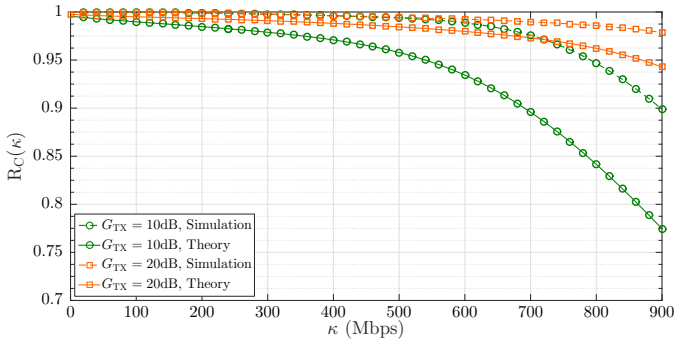

Fig. 7. Rate coverage probability R_C as a function of the threshold κ, for $\psi = 30°$, $G_{TX} = \{10\,\text{dB}, 20\,\text{dB}\}$, $\lambda_{BS} = 4 \cdot 10^{-3}$ and $N_o = 2$.

$\theta = 15\,\text{dB}$ or $25\,\text{dB}$, and $\psi = 30°$. In particular, as also shown in Fig. 4 and Fig. 5, as θ increases the deviation between the simulations and the theoretical model increases. However, the MSE between theory and simulation never exceeds $7.3 \cdot 10^{-3}$ in Figs. 5a and 5b.

Most importantly, Fig. 6 further reinforces what was already observed in Fig. 4 and Fig. 5:

- As expected, P_T increases as N_o increases. However, when N_o passes from 1 to 2, P_T increases no more than $8.6 \cdot 10^{-3}$. Hence, we conclude that the network is particularly resilient to the number of obstacle lanes.
- The impact of λ_{BS} on the value of P_T is reasonably small, if compared to what happens in a typical bi-dimensional mmWave cellular network [27]. This can be justified by the same reasoning provided for Fig. 4a.

Let us consider again Fig. 6; it shows that P_T has only trivial minimima for the considered values of θ. Specifically, for $\theta = 15\,\text{dB}$ and $\theta = 25\,\text{dB}$, if we refer only to the minimization of the SINR outage probability, the optimal value of λ_{BS} simply is $2 \cdot 10^{-4}$.

Remark 4.2: We observe that the most computational intense part in the derivation of the SINR outage probability is given by the numerical integration of functions involving $\mathcal{L}_I(s)$, as in (18) and (19). From Corollary 3.1 we have that $\mathcal{L}_I(s)$ is approximated as a product of terms based on the same expression, which involves the Gauss hypergeometric function ${}_2\tilde{F}_1(a, b; c; z)$. However, from (30), it follows that z is always a real number, which allows us to significantly reduce the complexity of the whole numerical integration process [48]. In fact, the computation of the theoretical values of P_T, for the values of θ considered in Figs. 4 and 5, takes just a few seconds[4].

Fig. 7 shows the rate coverage probability as a function of the rate threshold κ, for $\psi = 30°$, $\lambda_{BS} = 4 \cdot 10^{-3}$ and $N_o = 2$. From (24), we remark that the expression of R_C directly follows from P_T. For this reason, we observe that the greater the gain G_{TX}, the higher the value of R_C. Similarly, given the network resiliency to the increment of the number of obstacle lanes, the impact of N_o on the values of R_C is negligible.

[4]On a workstation equipped with an Intel Core i7 4790 (quad-core operating at 3.6 GHz) and 32 GB of RAM, the computational time was less than 10 s.

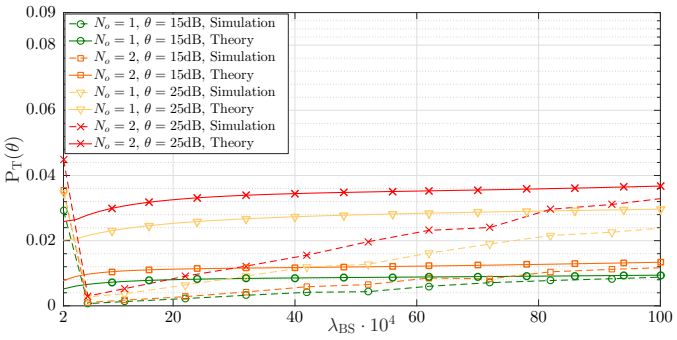

Fig. 8. SINR outage probability $\mathrm{P_T}$ as a function of the BS density λ_{BS}, for $\theta = \{15\,\mathrm{dB}, 25\,\mathrm{dB}\}$ dB, $N_o = \{1, 2\}$, $\psi = 30°$ and $G_{\mathrm{TX}} = 20\,\mathrm{dB}$. Simulation results obtained for $R = 20\,\mathrm{km}$ and the standard user placed at $(0, -w/2)$.

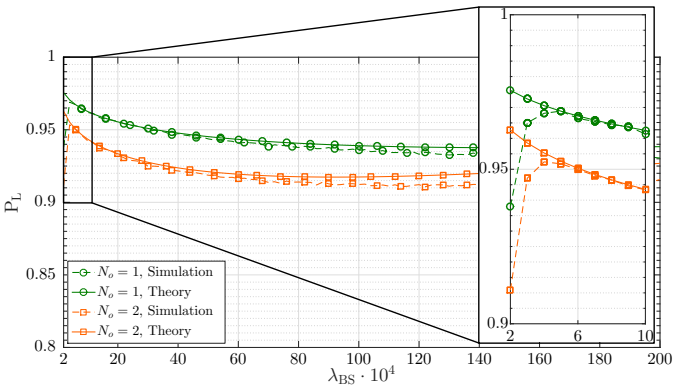

Fig. 9. Probability $\mathrm{P_L}$ that the standard users connects to a LOS BS as a function of λ_{BS}, for $N_o = 1$ and 2. Simulation results obtained for $R = 20\,\mathrm{km}$ and the standard user placed at $(0, -w/2)$.

Finally, we observe that the MSE between simulations and the proposed theoretical approximation is smaller than $3.5 \cdot 10^{-3}$.

For completeness, out model was validated by considering a significantly shorter highway section, namely $R = 20\,\mathrm{km}$. Without changing the proposed theoretical framework, our simulation model was run by assuming the standard user is placed in the middle of the lower-most user lane, which is $(0, -w/2)$. In particular, Fig. 8 compares simulation and theoretical results for the same transmission parameters and road layout as in Fig. 6. We observe that for $\lambda_{\mathrm{BS}} \geq 6 \cdot 10^{-4}$ simulation results are almost identical to those reported in Fig. 6, however there is a substantial deviation for $2 \cdot 10^{-4} \leq \lambda_{\mathrm{BS}} < 6 \cdot 10^{-4}$.

The aforementioned alteration can be easily explained by considering Fig. 9, which shows $\mathrm{P_L}$ as a function of λ_{BS} in the same simulated scenario as Fig. 8. Also, in this case, we observe that the simulation results overlap those as in Fig. 3 for $\lambda_{\mathrm{BS}} \geq 6 \cdot 10^{-4}$. However, once more there is a substantial deviation between theory and simulation for $\lambda_{\mathrm{BS}} < 6 \cdot 10^{-4}$, which has a direct impact on the results in Fig. 8. In particular, $\mathrm{P_L}$ appears to sharply decrease for very low BS densities, which is a clear side effect of considering small road sections. In fact, due to the small value of R, the simulated processes regulating the position of BSs and obstacles are no longer good approximations of the correspondent PPPs, for $\lambda_{\mathrm{BS}} < 6 \cdot 10^{-4}$. Despite that, we conclude that both Figs. 8 and 9 shows that the proposed theoretical model remains valid for $\lambda_{\mathrm{BS}} \geq 6 \cdot 10^{-4}$ for smaller road sections and in the case the standard user is located in the middle of a user lane.

V. Conclusions and Future Developments

This paper has addressed the issue of characterizing the downlink performance of a mmWave network deployed along a highway section. In particular, we proposed a novel theoretical framework for characterizing the SINR outage probability and rate coverage probability of a user surrounded by large vehicles sharing the other highway lanes. Our model treated large vehicles as blockages, and hence they impact on the considered LOS/NLOS model. One of the prominent features of our system model is that BSs are systematically placed at the side of the road, and large-footprint vehicles are assumed to drive along parallel lanes. Hence, unlike a typical stochastic geometry system, we assumed that both BS and blockage positions are governed by multiple independent mono-dimensional PPPs that are not independent to translations and rotations. This modelling choice allowed the proposed theoretical framework to model different road layouts.

We compared the proposed theoretical framework with simulation results, for a number of scenarios. In particular, we observed that the proposed theoretical framework can efficiently describe the network performance, in terms of SINR outage and rate coverage probability. Furthermore, we observed the following fundamental properties:

- The probability of being served by a NLOS BS is not negligible for practical system parameters.
- Reducing the antenna beamwidth from 90° to 30° does not necessarily have a disruptive impact on the SINR outage probability, and hence, on the rate coverage probability.
- In contrast with bi-dimensional mmWave cellular networks, the BS density does not strongly affect the network performance.
- Overall, for a fixed SINR threshold, the SINR outage probability is minimized by low BS densities, corresponding to sparse network deployments.

In the future, we plan to extend the characterization of the blockage distribution with the objective of taking into account heterogeneous traffic patterns. Furthermore, we plan to extend the proposed model by making it able to characterize mmWave vehicular communications in urban and suburban environments with irregular road layouts.

APPENDIX A
PROOF OF THEOREM 3.1

For $\mathbb{E}_1 = \{\mathrm{L}, \mathrm{N}\}$, the Laplace transform of $\mathrm{I}_{\mathrm{S,E}}$ can be expressed as:

$$\mathcal{L}_{\mathrm{I}_{\mathrm{S,E}},\mathbb{E}_1}(s) = \mathbb{E}_{\Phi_{\mathrm{S,E}}}\left(\prod_{j\in\Phi_{\mathrm{S,E}}} \mathbb{E}_h\mathbb{E}_\Delta\left(e^{-s|h_j|^2\Delta_j \ell(r_j)}\right)\right) \quad (25)$$

$$\overset{(i)}{=} \exp\left(-\mathbb{E}_\Delta\mathbb{E}_h \int_{w(N_o+1)}^{+\infty} e^{-sh\Delta r^{-\alpha_{\mathrm{E}}}} \cdot \frac{2rq\lambda_{\mathrm{E}}}{\sqrt{r^2 - w^2(N_o+1)^2}}\, dr\right) \quad (26)$$

where $\mathbb{E}_{\Phi_{\mathrm{S,E}}}$ represents the expectation with respect to the distance of each BS in $\Phi_{\mathrm{S,E}}$ from O. Similarly, operators $\mathbb{E}_\Delta$ and $\mathbb{E}_h$ signify the expectation with respect to the overall antenna gain and the small-scale fading gain associated with the transmissions of each BS, respectively. We observe that equality (i) arises from the use of the definition of the probability generating functional (pgfl) of a PPP [40, Definition 4.3] and the mapping theorem applied to $\Phi_{\mathrm{S,E}}$ [40, Theorem 2.34]. In addition, the pgfl allows us to drop the relation to a specific BS j in the terms expressing a distance of a BS to O, its channel and antenna gains. For this reason, in the integrand function, we simply refer to terms r, h and Δ.

Let a and b be two real numbers greater than or equal to $w(N_o+1)$ and such that $a \leq b$. With regards to (26), we condition with respect to a specific value of h and Δ, and we approximate the following term[5]:

$$\int_a^b e^{-sh\Delta r^{-\alpha_{\mathrm{E}}}} \frac{2rq\lambda_{\mathrm{E}}}{\sqrt{r^2 - w^2(N_o+1)^2}}\, dr$$

$$\overset{(i)}{=} \int_{\sqrt{a^2-w^2(N_o+1)^2}}^{\sqrt{b^2-w^2(N_o+1)^2}} e^{-sh\Delta(t^2+w^2(N_o+1)^2)^{-\alpha_{\mathrm{E}}/2}} 2q\lambda_{\mathrm{E}}\, dt$$

$$\overset{(ii)}{\cong} \int_a^b e^{-sh\Delta t^{-\alpha_{\mathrm{E}}}} 2q\lambda_{\mathrm{E}}\, dt \quad (27)$$

$$\overset{(iii)}{=} -2q\lambda_{\mathrm{E}} \int_{a^{-\alpha_{\mathrm{E}}}}^{b^{-\alpha_{\mathrm{E}}}} (1 - e^{-sh\Delta x})\alpha_{\mathrm{E}}^{-1} x^{-\alpha_{\mathrm{E}}^{-1}-1}\, dx$$

$$\overset{(iv)}{=} \overbrace{2q\lambda_{\mathrm{E}}\left[(1-e^{-sh\Delta x})x^{-\alpha_{\mathrm{E}}^{-1}}\right]_{x=a^{-\alpha_{\mathrm{E}}}}^{b^{-\alpha_{\mathrm{E}}}}}^{\Theta(h,\Delta)} \underbrace{-2q\lambda_{\mathrm{E}} \int_{a^{-\alpha_{\mathrm{E}}}}^{b^{-\alpha_{\mathrm{E}}}} sh\Delta x^{-\frac{1}{\alpha_{\mathrm{E}}}} e^{-sh\Delta x}\, dx}_{\Lambda(h,\Delta)}, \quad (28)$$

where (i) arises from the change of variable $t \leftarrow \sqrt{r^2 - w^2(N_o+1)^2}$, while (ii) assumes that $w(N_o+1)$ is equal to 0 (see Section IV-B for the validation of the proposed theoretical framework). Equality (iii) arises by applying the changes of variable $y \leftarrow t^{\alpha_{\mathrm{E}}}$ and then $x \leftarrow y^{-1}$. In addition, in (iv), we resort to an integration by parts.

With regards to (28), we keep the conditioning to Δ and calculate the expectation of $\Theta(h,\Delta)$ and $\Lambda(h,\Delta)$, with respect to h. From Assumption 3.1, it should be noted that we refer to a Rayleigh channel model, and, hence, the following relation holds:

$$\mathbb{E}_h\left[\Theta(h,\Delta)\right] = 2q\lambda_{\mathrm{E}}\left[x^{-\alpha_{\mathrm{E}}^{-1}}\left(1 - \frac{1}{s\Delta x+1}\right)\right]_{x=a^{-\alpha_{\mathrm{E}}}}^{b^{-\alpha_{\mathrm{E}}}}. \quad (29)$$

Term $\mathbb{E}_h\left[\Lambda(h,\Delta)\right]$ can be found as follows:

$$\mathbb{E}_h\left[\Lambda(h,\Delta)\right] = -2q\lambda_{\mathrm{E}} \int_{a^{-\alpha_{\mathrm{E}}}}^{b^{-\alpha_{\mathrm{E}}}} x^{-\frac{1}{\alpha_{\mathrm{E}}}} \cdot \int_0^\infty sh\Delta e^{-(s\Delta x+1)h}\, dh\, dx \quad (30)$$

$$= -2q\lambda_{\mathrm{E}} \int_{a^{-\alpha_{\mathrm{E}}}}^{b^{-\alpha_{\mathrm{E}}}} x^{-\frac{1}{\alpha_{\mathrm{E}}}} \frac{\partial}{\partial x}\left(-\frac{1}{s\Delta x+1}\right) dx$$

$$\overset{(i)}{=} -2q\lambda_{\mathrm{E}}(s\Delta)^{\frac{1}{\alpha_{\mathrm{E}}}} \int_{-(s\Delta a^{-\alpha_{\mathrm{E}}}+1)^{-1}}^{-(s\Delta b^{-\alpha_{\mathrm{E}}}+1)^{-1}} \left(-\frac{1}{t} - 1\right)^{-\frac{1}{\alpha_{\mathrm{E}}}} dt$$

$$\overset{(ii)}{=} -2q\lambda_{\mathrm{E}}(s\Delta)^{\frac{1}{\alpha_{\mathrm{E}}}} \left[t(-t^{-1})^{-\frac{1}{\alpha_{\mathrm{E}}}}\Gamma\left(\frac{1}{\alpha_{\mathrm{E}}}+1\right) \cdot {}_2\tilde{F}_1\left(\frac{1}{\alpha_{\mathrm{E}}}, \frac{1}{\alpha_{\mathrm{E}}}+1; \frac{1}{\alpha_{\mathrm{E}}}+2; -t\right)\right]_{t=-(s\Delta a^{-\alpha_{\mathrm{E}}}+1)^{-1}}^{-(s\Delta b^{-\alpha_{\mathrm{E}}}+1)^{-1}},$$

where (i) arises from the change of variable $t \leftarrow -\frac{1}{s\Delta x+1}$. Let us signify with ${}_2\tilde{F}_1(a,b;c;z) = \sum_{k=0}^{\infty} \frac{\{a\}_k\{b\}_k}{\{c\}_k}\frac{z^k}{k!}$ the Gauss hypergeometric function. We observe that the integral as in equality (i) is closely related to that as in [49, Eq. (3.228.3)], and after some manipulations we have equality (ii).

From the approximation in (27), it follows that $a \cong \sqrt{a^2 - w^2(N_o+1)^2}$ and $b \cong \sqrt{b^2 - w^2(N_o+1)^2}$. Hence, we observe that $\mathcal{L}_{\mathrm{I}_{\mathrm{S,E}},\mathbb{E}_1}(s)$, conditioned on the gain Δ (see (9)), can be expressed as follows:

$$\mathcal{L}_{\mathrm{I}_{\mathrm{S,E}},\mathbb{E}_1}(s) \cong \mathcal{L}_{\mathrm{I}_{\mathrm{S,E}},\mathbb{E}_1}(s;a,b,\Delta)\Big|_{a=0,b=+\infty} \quad (31)$$

$$= \exp\left(-\left(\mathbb{E}_h[\Theta(h,\Delta)] + \mathbb{E}_h[\Lambda(h,\Delta)]\Big|_{a=0,b=+\infty}\right)\right).$$

Let us focus on the transmit antenna gain of the j-th interfering BS, which has a PDF that depends on the distance r_j and the orientation of the beam ϵ_i. Unfortunately, to take into account the exact formulation of the aforementioned PDF would make the performance model intractable. As such, we instead make the approximation that the transmit antenna gain is always equal to g_{TX}. Our approximation via simulation is validated in Section IV-B.

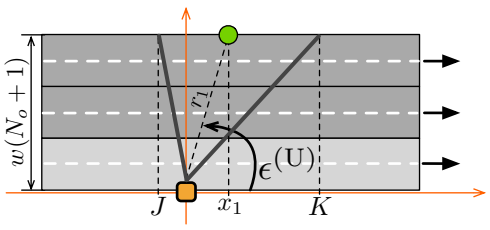

Fig. 10. Case where the standard user is served by a BS from the upper side of the road.

[5]For clarity, we define $[f(x)]_{x=a}^{b} = f(b) - f(a)$.

With regards to (25), we observe that after conditioning on the standard user being connected to a BS at a distance r_1 from O, then the receive antenna gain g of the interfering BSs j is determined by the parameter list $< |x_1|, p, r, \mathbb{S}_1, \mathbb{E}_1, \mathrm{S}, \mathrm{E} >$, where: (i) $|x_1|$ is the absolute value of the x-axis coordinate of BS 1, (ii) p captures the fact that the interfering BS is at a location on the positive (right-hand side of y-axis, RX) or negative side (left-hand side of y-axis, LX) of the x-axis, and (iii) r is the distance of the interfering BS to O.

Let us consider the x-axis coordinates J and K of the points where the two rays defining the antenna beam of the standard user intersect the side of the road, as shown in Fig. 10. The receive antenna gain of the interfering BS also depends on: (i) the fact the standard user connects to a BS on the upper/bottom side of the road ($\mathbb{S}_1 \in \{\mathrm{U}, \mathrm{B}\}$), that can be in LOS/NLOS ($\mathbb{E}_1 \in \{\mathrm{L}, \mathrm{N}\}$) with respect to the standard user, (ii) the values of S and E, and (iii) the specific configuration of the values of $|x_1|$, J and K. By invoking the same approximation as in (27), we say that $r \cong \sqrt{r^2 - w^2(N_o+1)^2}$ and the following parameters determine the receiver gain:

- $\mathbb{S}_1 = \mathrm{U}$, $\mathbb{E}_1 = \mathrm{L}$, $\mathrm{S} = \mathrm{U}$ and $\mathrm{E} = \mathrm{L}$ - we divide this case into the following subcases:
  - If the value of $|x_1|$ is such that $J > 0$ - we observe that that there are no LOS BSs at a distance smaller than $|x_1|$. Hence, it follows that

$$g = G_{\mathrm{RX}} \quad \text{if} \quad \begin{cases} |x_1| \leq r \leq K \\ p = \mathrm{RX} \end{cases} \tag{32}$$

$$g = g_{\mathrm{RX}} \quad \text{if} \quad \begin{cases} K \leq r \leq +\infty \\ p = \mathrm{RX} \end{cases} \text{ or } \begin{cases} |x_1| \leq r \leq +\infty \\ p = \mathrm{LX} \end{cases} \tag{33}$$

  - If $J \leq 0$ - by following the same reasoning as before, in addition to the case as in (32), it follows that

$$g = g_{\mathrm{RX}} \quad \text{if} \quad \begin{cases} K \leq r \leq +\infty \\ p = \mathrm{RX} \end{cases} \text{ or } \begin{cases} |J| \leq r \leq +\infty \\ p = \mathrm{LX} \end{cases} \tag{34}$$

$$g = G_{\mathrm{RX}} \quad \text{if} \quad \begin{cases} |x_1| \leq r \leq |J| \\ p = \mathrm{LX} \end{cases} \tag{35}$$

- $\mathbb{S}_1 = \mathrm{U}$, $\mathbb{E}_1 = \mathrm{L}$, $\mathrm{S} = \mathrm{U}$ and $\mathrm{E} = \mathrm{N}$ - we apply the same reasoning as before by bearing in mind that it is impossible for a NLOS BS to be at a distance that is smaller than $\mathrm{A_N}(r_1)$ to O. Equivalently, it is impossible for a NLOS BS to be associated with a x-axis coordinate smaller than $x_{\mathrm{N}}(r_1) = \sqrt{(\mathrm{A_N}(r_1))^2 - w^2(N_o+1)^2}$. In particular, for $J \leq 0$, the value of g can be derived as in (32) and (34)-(35), where term $|x_1|$ is replaced by $x_{\mathrm{N}}(r_1)$. On the other hand, for $J > 0$, the value of g can be expressed as follows:

$$g = g_{\mathrm{RX}} \quad \text{if} \quad \begin{cases} x_{\mathrm{N}}(r_1) \leq r \leq J \text{ or } K \leq r \leq +\infty \\ p = \mathrm{RX} \end{cases} \text{ or } \begin{cases} x_{\mathrm{N}}(r_1) \leq r \leq +\infty \\ p = \mathrm{LX} \end{cases} \tag{36}$$

$$g = G_{\mathrm{RX}} \quad \text{if} \quad \begin{cases} J \leq r \leq K \\ p = \mathrm{RX} \end{cases} \tag{37}$$

- $\mathbb{S}_1 = \mathrm{U}$, $\mathbb{E}_1 = \mathrm{L}$, $\mathrm{S} = \mathrm{B}$ and $\mathrm{E} = \mathrm{L}$ - from Assumption 2.7, we observe that g is always equal to g_{RX}. In addition, we note that it is not possible to have a LOS BS at a distance smaller than r_1. Hence, we have only two possible configurations:

$$g = g_{\mathrm{RX}} \quad \text{if} \quad \begin{cases} |x_1| \leq r \leq +\infty \\ p = \mathrm{RX} \end{cases} \text{ or } \begin{cases} |x_1| \leq r \leq +\infty \\ p = \mathrm{LX} \end{cases} \tag{38}$$

- $\mathbb{S}_1 = \mathrm{U}$, $\mathbb{E}_1 = \mathrm{L}$, $\mathrm{S} = \mathrm{B}$ and $\mathrm{E} = \mathrm{N}$ - similarly to the previous case, we observe that g is equal to g_{RX} and it is not possible to have a NLOS BS at a distance smaller than $x_{\mathrm{N}}(r_1)$. Hence, we have the following cases:

$$g = g_{\mathrm{RX}} \quad \text{if} \quad \begin{cases} x_{\mathrm{N}}(r_1) \leq r \leq +\infty \\ p = \mathrm{RX} \end{cases} \text{ or } \begin{cases} x_{\mathrm{N}}(r_1) \leq r \leq +\infty \\ p = \mathrm{LX} \end{cases} \tag{39}$$

- With regards the remaining parameter combinations where $\mathbb{S}_1 = \mathrm{U}$, $\mathbb{E}_1 = \mathrm{N}$, we observe the following cases:
  - $\mathrm{S} = \mathrm{U}$, $\mathrm{E} = \mathrm{L}$ - we define $x_{\mathrm{L}}(r_1) = \sqrt{(\mathrm{A_L}(r_1))^2 - w^2(N_o+1)^2}$. If $x_{\mathrm{L}}(r_1) > K$, refer to (38) and replace $|x_1|$ with $x_{\mathrm{L}}(r_1)$. Otherwise, refer to (32)-(35) and replace $|x_1|$ with $x_{\mathrm{L}}(r_1)$.
  - $\mathrm{S} = \mathrm{U}$, $\mathrm{E} = \mathrm{N}$ - refer to (32)-(35).
  - $\mathrm{S} = \mathrm{B}$, $\mathrm{E} = \mathrm{L}$ - refer to (38) and replace $|x_1|$ with $x_{\mathrm{L}}(r_1)$.
  - $\mathrm{S} = \mathrm{B}$, $\mathrm{E} = \mathrm{N}$ - refer to (38).
- By following the above approach, it is possible to derive all the remaining configurations. In particular, the characterization of g, for a parameter configuration where $\mathbb{S}_1 = \mathrm{B}$ and $\mathrm{S} = \mathrm{B}$ ($\mathbb{S}_1 = \mathrm{B}$ and $\mathrm{S} = \mathrm{U}$) follows exactly the same rule of the corespondent parameter list, where $\mathbb{S}_1 = \mathrm{U}$ and $\mathrm{S} = \mathrm{U}$ ($\mathbb{S}_1 = \mathrm{U}$ and $\mathrm{S} = \mathrm{B}$).

The aforementioned parameter configurations are also summarized in Table III. With regards to parameter p, we observe that the probability $\mathbb{P}[p]$ of p being equal to DX or RX is $1/2$.

Consider (31), all the elements are in place to explicitly calculate the expectation with respect to Δ. In particular, it follows that the final $\mathcal{L}_{\mathrm{I_{S,E}}}(s)$ can be expressed as:

$$\begin{aligned}
\mathcal{L}_{\mathrm{I_{S,E,\mathbb{E}_1}}}(s) &\overset{(i)}{\cong} \exp\left(-\mathbb{E}_\Delta\left(\mathbb{E}_h[\Theta(h,\Delta)+\Lambda(h,\Delta)]\Big|_{a=0,b=+\infty}\right)\right) \\
&\overset{(ii)}{\cong} \exp\left(-\sum_{\substack{\mathbb{S}_1\in\{\mathrm{U,B}\} \\ (a,b,\Delta)\in\mathcal{C}_{|\mathrm{x_1}|,\mathbb{S}_1,\mathbb{E}_1,\mathrm{S,E}}}} \mathbb{P}[p]\left(\mathbb{E}_h[\Theta(h,\Delta)+\Lambda(h,\Delta)]\Big|_{a,b,\Delta}\right)\right) \\
&= \prod_{\substack{\mathbb{S}_1\in\{\mathrm{U,B}\}, \\ (a,b,\Delta)\in\mathcal{C}_{|\mathrm{x_1}|,\mathbb{S}_1,\mathbb{E}_1,\mathrm{S,E}}}} \exp\left(-\frac{1}{2}\left(\mathbb{E}_h[\Theta(h,\Delta)]\Big|_{a,b,\Delta} + \mathbb{E}_h[\Lambda(h,\Delta)]\Big|_{a,b,\Delta}\right)\right) \\
&= \prod_{\substack{\mathbb{S}_1\in\{\mathrm{U,B}\}, \\ (a,b,\Delta)\in\mathcal{C}_{|\mathrm{x_1}|,\mathbb{S}_1,\mathbb{E}_1,\mathrm{S,E}}}} \sqrt{\mathcal{L}_{\mathrm{I_{S,E},\mathbb{E}_1}}(s;a,b,\Delta)},
\end{aligned} \tag{40}$$

where (i) is (31). From the previous discussion, for a given $|x_1|$, Δ can either be equal to $g_{\mathrm{TX}}g_{\mathrm{RX}}$ or $g_{\mathrm{TX}}G_{\mathrm{RX}}$. In particular, the value of Δ is determined by the list of parameters $< \mathrm{x_1}, \mathbb{S}_1, \mathbb{E}_1, \mathrm{S}, \mathrm{E} >$, where terms a and b are the minimum and maximum distance r to an interfering BS, respectively. We define sequence $\mathcal{C}_{|\mathrm{x_1}|,\mathbb{S}_1,\mathbb{E}_1,\mathrm{S,E}}$. This sequence consists of all the possible parameter configurations (a,b,Δ). For

instance, if $\mathbb{S}_1 = \mathrm{U}$, $\mathbb{E}_1 = \mathrm{L}$, $\mathrm{S} = \mathrm{U}$, $\mathrm{E} = \mathrm{L}$ and $J > 0$, sequence $\mathcal{C}_{|\mathrm{x}_1|,\mathbb{S}_1,\mathbb{E}_1,\mathrm{S},\mathrm{E}}$ consists of: $(|x_1|, K, g_{\mathrm{TX}}G_{\mathrm{RX}})$, $(K, +\infty, g_{\mathrm{TX}}g_{\mathrm{RX}})$ and $(|x_1|, +\infty, g_{\mathrm{TX}}g_{\mathrm{RX}})$. We note that each element of a sequence $\mathcal{C}_{|\mathrm{x}_1|,\mathbb{S}_1,\mathbb{E}_1,\mathrm{S},\mathrm{E}}$ occurs with probability $\mathbb{P}[p]$. Furthermore, we observe that like those in (38) and (39), sequence $\mathcal{C}_{|\mathrm{x}_1|,\mathbb{S}_1,\mathbb{E}_1,\mathrm{S},\mathrm{E}}$ lists twice the same parameter configuration. Given these reasons, the term $\mathbb{E}_\Delta(\mathbb{E}_h[\Theta(h,\Delta) + \Lambda(h,\Delta)]\big|_{a=0,b=+\infty})$ can be approximated as in (ii). After some manipulations of approximation (ii), we get to (11), which concludes the proof.

REFERENCES

[1] D. Evans, "The Internet of Things," Cisco IBSG, Tech. Rep., Apr. 2011. [Online]. Available: https://www.cisco.com/c/dam/en_us/about/ac79/docs/innov/IoT_IBSG_0411FINAL.pdf

[2] "10 Million Self-Driving Cars will be on the Road by 2020," Business Insider UK, Tech. Rep., Jun. 2016. [Online]. Available: http://uk.businessinsider.com/report-10-million-self-driving-cars-will-be-on-the-road-by-2020-2015-5-6

[3] "Preliminary Statement of Policy Concerning Automated Vehicles," U.S. Department of Transportation, National Highway Traffic Safety Administration (NHTSA), Tech. Rep., 2013. [Online]. Available: http://www.nhtsa.gov/staticfiles/rulemaking/pdf/Automated_Vehicles_Policy.pdf

[4] "C-ITS Platform," European Commission, Tech. Rep., Jan. 2016. [Online]. Available: http://ec.europa.eu/transport/themes/its/doc/c-its-platform-final-report-january-2016.pdf

[5] "J3016: Taxonomy and Definitions for Terms Related to On-Road Motor Vehicle Automated Driving Systems," SAE, Tech. Rep., Jan. 2014. [Online]. Available: http://standards.sae.org/j3016_201401/

[6] "5G-PPP White Paper on Automotive Vertical Sector," 5G Infrastructure Public Private Partnership, Tech. Rep., Oct. 2015. [Online]. Available: https://5g-ppp.eu/wp-content/uploads/2014/02/5G-PPP-White-Paper-on-Automotive-Vertical-Sectors.pdf

[7] N. Lu, N. Cheng, N. Zhang, X. Shen, and J. W. Mark, "Connected Vehicles: Solutions and Challenges," *IEEE Internet Things J.*, vol. 1, no. 4, pp. 289–299, Aug. 2014.

[8] E. Uhlemann, "Connected-Vehicles Applications Are Emerging," *IEEE Veh. Technol. Mag.*, vol. 11, no. 1, pp. 25–96, Mar. 2016.

[9] J. Choi, N. G. Prelcic, R. C. Daniels, C. R. Bhat, and R. W. Heath Jr., "Millimeter Wave Vehicular Communication to Support Massive Automotive Sensing," *submitted to IEEE Commun. Mag.*, Mar. 2016. [Online]. Available: http://arxiv.org/abs/1602.06456

[10] J. B. Kenney, "Dedicated Short-Range Communications (DSRC) Standards in the United States," *Proceedings of the IEEE*, vol. 99, no. 7, pp. 1162–1182, Jul. 2011.

[11] G. Karagiannis, O. Altintas, E. Ekici, G. Heijenk, B. Jarupan, K. Lin, and T. Weil, "Vehicular Networking: A Survey and Tutorial on Requirements, Architectures, Challenges, Standards and Solutions," *IEEE Commun. Surveys Tuts.*, vol. 13, no. 4, pp. 584–616, Fourth 2011.

[12] E. Uhlemann, "Introducing Connected Vehicles," *IEEE Veh. Technol. Mag.*, vol. 10, no. 1, pp. 23–31, Mar. 2015.

[13] E. G. Strom, "On Medium Access and Physical Layer Standards for Cooperative Intelligent Transport Systems in Europe," *Proceedings of the IEEE*, vol. 99, no. 7, pp. 1183–1188, Jul. 2011.

[14] M. Xie, Y. Shang, Z. Yang, Y. Jing, and H. Zhou, "A Novel MBSFN Scheme for Vehicle-to-Vehicle Safety Communication Based on LTE Network," in *Proc. of IEEE VTC-Fall 2015*, Boston, Massachusetts, USA, Sep. 2015, pp. 1–5.

[15] G. Araniti, C. Campolo, M. Condoluci, A. Iera, and A. Molinaro, "LTE for Vehicular Networking: A Survey," *IEEE Commun. Mag.*, vol. 51, no. 5, pp. 148–157, May 2013.

[16] T. Nitsche, C. Cordeiro, A. B. Flores, E. W. Knightly, E. Perahia, and J. C. Widmer, "IEEE 802.11ad: Directional 60 GHz Communication For Multi-Gigabit-per-Second Wi-Fi," *IEEE Commun. Mag.*, vol. 52, no. 12, pp. 132–141, Dec. 2014.

[17] J. G. Andrews, S. Buzzi, W. Choi, S. V. Hanly, A. Lozano, A. C. K. Soong, and J. C. Zhang, "What Will 5G Be?" *IEEE J. Sel. Areas Commun.*, vol. 32, no. 6, pp. 1065–1082, Jun. 2014.

[18] T. S. Rappaport, F. Gutierrez, E. Ben-Dor, J. N. Murdock, Y. Qiao, and J. I. Tamir, "Broadband Millimeter-Wave Propagation Measurements and Models Using Adaptive-Beam Antennas for Outdoor Urban Cellular Communications," *IEEE Trans. Antennas Propag.*, vol. 61, no. 4, pp. 1850–1859, Apr. 2013.

[19] T. Rappaport, R. Heath, R. Daniels, and J. Murdock, *Millimeter Wave Wireless Communications*, ser. Communication engineering and emerging technologies. Prentice Hall, 2014.

[20] J. Gozalves, "Fifth-Generation Technologies Trials," *IEEE Veh. Technol. Mag.*, vol. 11, no. 2, pp. 5–13, Jun. 2016.

[21] S. Hasan, N. Siddique, and S. Chakraborty, *Intelligent Transport Systems: 802.11-based Roadside-to-Vehicle Communications*. Springer New York, 2012.

[22] C. Lochert, B. Scheuermann, C. Wewetzer, A. Luebke, and M. Mauve, "Data Aggregation and Roadside Unit Placement for a VANET Traffic Information System," in *Proc. of the fifth ACM international workshop on VehiculAr Inter-NETworking*, San Francisco, California, USA, 2008, pp. 58–65.

[23] O. Trullols, M. Fiore, C. Casetti, C. Chiasserini, and J. B. Ordinas, "Planning roadside infrastructure for information dissemination in intelligent transportation systems," *ELSEVIER Computer Communications*, vol. 33, no. 4, pp. 432 – 442, 2010.

[24] A. Ghosh, T. A. Thomas, M. C. Cudak, R. Ratasuk, P. Moorut, F. W. Vook, T. S. Rappaport, G. R. MacCartney, S. Sun, and S. Nie, "Millimeter-Wave Enhanced Local Area Systems: A High-Data-Rate Approach for Future Wireless Networks," *IEEE J. Sel. Areas Commun.*, vol. 32, no. 6, pp. 1152–1163, Jun. 2014.

[25] G. Zhang, T. Q. S. Quek, M. Kountouris, A. Huang, and H. Shan, "Fundamentals of Heterogeneous Backhaul Design - Analysis and Optimization," *IEEE Trans. Commun.*, vol. 64, no. 2, pp. 876–889, Feb. 2016.

[26] S. Singh, M. N. Kulkarni, A. Ghosh, and J. G. Andrews, "Tractable Model for Rate in Self-Backhauled Millimeter Wave Cellular Networks," *IEEE J. Sel. Areas Commun.*, vol. 33, no. 10, pp. 2196–2211, Oct. 2015.

[27] T. Bai and R. W. Heath Jr., "Coverage and Rate Analysis for Millimeter-Wave Cellular Networks," *IEEE Trans. Wireless Commun.*, vol. 14, no. 2, pp. 1100–1114, Feb. 2015.

[28] R. Baldemair, T. Irnich, K. Balachandran, E. Dahlman, G. Mildh, Y. Selén, S. Parkvall, M. Meyer, and A. Osseiran, "Ultra-Dense Networks in Millimeter-Wave Frequencies," *IEEE Commun. Mag.*, vol. 53, no. 1, pp. 202–208, Jan. 2015.

[29] M. D. Renzo, "Stochastic Geometry Modeling and Analysis of Multi-Tier Millimeter Wave Cellular Networks," *IEEE Trans. Wireless Commun.*, vol. 14, no. 9, pp. 5038–5057, Sep. 2015.

[30] S. Takahashi, A. Kato, K. Sato, and M. Fujise, "Distance Dependence of Path Loss for Millimeter Wave Inter-Vehicle Communications," in *Proc. of IEEE VTC 2003-Fall*, vol. 1, Orlando, Florida, USA, Oct. 2003, pp. 26–30.

[31] M. Haenggi, J. G. Andrews, F. Baccelli, O. Dousse, and M. Franceschetti, "Stochastic Geometry and Random Graphs for the Analysis and Design of Wireless Networks," *IEEE J. Sel. Areas Commun.*, vol. 27, no. 7, pp. 1029–1046, Sep. 2009.

[32] S. P. Weber, X. Yang, J. G. Andrews, and G. de Veciana, "Transmission Capacity of Wireless Ad-Hoc Networks with Outage Constraints," *IEEE Trans. Inf. Theory*, vol. 51, no. 12, pp. 4091–4102, Dec. 2005.

[33] C.-H. Lee, C.-Y. Shih, and Y.-S. Chen, "Stochastic Geometry Based Models for Modeling Cellular Networks in Urban," *Springer Wireless Networks*, vol. 19, no. 6, pp. 1063–1072, 2013.

[34] H. ElSawy, E. Hossain, and M. Haenggi, "Stochastic Geometry for Modeling, Analysis, and Design of Multi-Tier and Cognitive Cellular Wireless Networks: A Survey," *IEEE Commun. Surveys Tuts.*, vol. 15, no. 3, pp. 996–1019, Third 2013.

[35] S. Singh, H. S. Dhillon, and J. G. Andrews, "Offloading in Heterogeneous Networks: Modeling, Analysis, and Design Insights," *IEEE Trans. Wireless Commun.*, vol. 12, no. 5, pp. 2484–2497, May 2013.

[36] A. B. Reis, S. Sargento, F. Neves, and O. Tonguz, "Deploying Roadside Units in Sparse Vehicular Networks: What Really Works and What Does Not," *IEEE Trans. Veh. Technol.*, vol. 63, no. 6, pp. 2794–2806, Jul. 2014.

[37] K. Rostamzadeh and S. Gopalakrishnan, "Analysis of Message Delivery Delay in Vehicular Networks," *IEEE Trans. Veh. Technol.*, vol. 64, no. 10, pp. 4770–4779, Oct. 2015.

[38] N. Akhtar, S. C. Ergen, and O. Ozkasap, "Vehicle Mobility and Communication Channel Models for Realistic and Efficient Highway VANET Simulation," *IEEE Trans. Veh. Technol.*, vol. 64, no. 1, pp. 248–262, Jan. 2015.

[39] M. J. Farooq, H. ElSawy, and M. S. Alouini, "A Stochastic Geometry Model for Multi-Hop Highway Vehicular Communication," *IEEE Trans. Wireless Commun.*, vol. 15, no. 3, pp. 2276–2291, Mar. 2016.
[40] M. Haenggi, *Stochastic Geometry for Wireless Networks*, ser. Stochastic Geometry for Wireless Networks. Cambridge University Press, 2013.
[41] D. Maamari, N. Devroye, and D. Tuninetti, "Coverage in mmWave Cellular Networks With Base Station Co-Operation," *IEEE Trans. Wireless Commun.*, vol. 15, no. 4, pp. 2981–2994, Apr. 2016.
[42] Z. Pi and F. Khan, "An introduction to millimeter-wave mobile broadband systems," *IEEE Commun. Mag.*, vol. 49, no. 6, pp. 101–107, Jun. 2011.
[43] P. Ioannou, *Automated Highway Systems*. Springer US, 2013.
[44] M. Abe, *The Dynamics of Vehicles on Roads and on Tracks Supplement to Vehicle System Dynamics: Proc. of the 18th IAVSD Symposium*, ser. Supplement to vehicle system dynamics. Taylor & Francis, 2005.
[45] "Proposed simulation framework and theoretical model." [Online]. Available: https://www.dropbox.com/s/r6wiuu01k0r0kt3/src.tar.bz2?dl=0
[46] M. Haenggi and R. K. Ganti, "Interference in Large Wireless Networks," *Foundations and Trends in Networking, Now Publishers*, vol. 3, no. 2, pp. 127–248, 2008.
[47] S. Weber and M. Kam, "Computational Complexity of Outage Probability Simulations in Mobile Ad-Hoc Networks," in *Proc. of the 39th Annual Conference on Information Sciences and Systems (CISS)*, Baltimore, Maryland, USA, Mar. 2005.
[48] R. K. S. Hankin, "Numerical evaluation of the Gauss hypergeometric function with the hypergeo package," *The R Journal*, vol. 7, no. 2, pp. 81–88, Dec. 2015.
[49] A. Jeffrey and D. Zwillinger, *Table of Integrals, Series, and Products*, ser. Table of Integrals, Series, and Products Series. Elsevier Science, 2007.